

doi: 10.12029/gc20200326002

陈俞宏,甘甜,管申进,赵剑星,孔志岗,邓明国. 2023. 滇西水头山岩浆热液铅锌矿床: 来自REE和C-O同位素的证据[J]. 中国地质, 50(3): 818–836.

Chen Yuhong, Gan Tian, Guan Shenjin, Zhao Jianxing, Kong Zhigang, Deng Mingguo. 2023. Shuitoushan magmatic hydrothermal lead-zinc deposit in western Yunnan: Evidence from REE and C-O isotopes[J]. Geology in China, 50(3): 818–836(in Chinese with English abstract).

# 滇西水头山岩浆热液铅锌矿床: 来自REE和C-O同位素的证据

陈俞宏<sup>1,2</sup>, 甘甜<sup>3,4</sup>, 管申进<sup>1</sup>, 赵剑星<sup>5</sup>, 孔志岗<sup>1,6</sup>, 邓明国<sup>1</sup>

(1. 昆明理工大学国土资源工程学院, 云南昆明 650093; 2. 云南省核工业二〇九地质大队, 云南昆明 650106; 3. 中国科学院地球化学研究所, 矿床地球化学国家重点实验室, 贵州贵阳 550081; 4. Department of Geosciences, College of Science, Virginia Tech, Blacksburg Virginia 24061, USA; 5. 广西地矿局二七一地质队, 广西桂林 541100; 6. 中国地质科学院矿产资源研究所, 北京 100037)

**提要:**【研究目的】位于西南“三江”成矿带保山地块南部的水头山矿床, 是镇康矿集区内新近勘查突破的又一典型的低温热液型 Pb-Zn 矿床, 由于矿区未出露岩浆岩, 矿床成因存在争议, 本文旨在通过对其成矿物质、成矿流体来源的研究, 厘定该矿床成因类型。【研究方法】在详细划分该矿床成矿期次和成矿阶段的基础上, 运用电感耦合等离子体质谱仪(ICP-MS)对该矿床岩(矿)石和不同阶段的硫化物进行了系统的稀土元素分析, 对赋矿围岩碳酸盐岩、大理岩及不同期次的方解石开展了 C-O 同位素地球化学组成研究, 并与毗邻的芦子园超大型铅锌铁多金属矿床进行综合对比, 探讨水头山矿床成矿物质来源及成矿流体特征, 揭示矿床的成矿机理。【研究结果】该矿床成矿作用可划分为成矿期和表生期, 其中热液成矿期可划分为阶段 I (黄铁矿-黄铜矿-方解石阶段)、阶段 II (闪锌矿-方铅矿-方解石阶段) 和阶段 III (黄铜矿-方解石阶段)。稀土元素及 C-O 同位素组成特征的研究表明, 水头山矿床各成矿阶段单矿物、矿石 Y/Ho 值显示其成矿物质来源与深部岩浆活动有关; 通过对该矿床单矿物、矿石稀土元素配分模式与保山地块内燕山期的柯街、志本山花岗岩体的稀土配分模式分析对比, 表明该矿床成矿流体中的 REE 主要来自深部岩浆热液,  $\delta^{13}\text{C}_{\text{V}-\text{PDB}}-\delta^{18}\text{O}_{\text{V}-\text{SMOW}}$  图解显示其成矿流体也主要来自岩浆热液, 前期成矿热液运移中有沉积岩的混染, 后期可能受低温蚀变作用与大气降水的影响。【结论】水头山矿床无论是成矿物质还是成矿流体来源均与矿区深部的岩浆热液密切相关, 且与毗邻的芦子园超大型 Pb-Zn-Fe 多金属矿床具有同源性, 是与深部中酸性岩浆热液有关的浅成低温热液矿床。

**关 键 词:**Pb-Zn 矿床; 稀土元素; C-O 同位素; 成矿物质来源; 矿产勘查工程; 水头山; 保山地块; 云南

**创 新 点:**查明了水头山 Pb-Zn 矿床的成矿流体特征及成矿物质来源, 揭示了保山地块镇康矿集区内芦子园超大型矽卡岩型 Pb-Zn-Fe 矿床与外围低温热液型水头山 Pb-Zn 矿床的成矿流体和成矿物质来源具有同源性, 是与深部中酸性岩浆作用有关的同一成矿系统的产物, 为区域矿床学研究以及铅锌矿床成矿规律总结提供了科学支撑。

中图分类号:P618.42; P618.43 文献标志码:A 文章编号:1000-3657(2023)03-0818-19

收稿日期:2020-03-26; 改回日期:2020-06-01

基金项目:国家自然科学基金项目(41363001、41762009)资助。

作者简介:陈俞宏,男,1995年生,硕士,助理工程师,主要从事扩矿勘探和矿床地质研究;E-mail: 630476104@qq.com。

通讯作者:赵剑星,男,1988年生,工程师,从事找矿勘探和矿床地质研究;E-mail: 1770733128@qq.com。

## Shuitoushan magmatic hydrothermal lead-zinc deposit in western Yunnan: Evidence from REE and C–O isotopes

CHEN Yuhong<sup>1,2</sup>, GAN Tian<sup>3,4</sup>, GUAN Shenjin<sup>1</sup>, ZHAO Jianxing<sup>5</sup>,  
KONG Zhigang<sup>1,6</sup>, DENG Mingguo<sup>1</sup>

(1. Faculty of Land Resource Engineering, Kunming University of Science and Technology, Kunming 650093, Yunnan, China;  
2. No.209 Geological Brigade, Geological Bureau of Yunnan Nuclear Industry, Kunming 650106, Yunnan, China; 3. Stake Key  
Laboratory of Ore Deposit Geochemistry, Institute of Geochemistry, Chinese Academy Sciences, Guiyang 550081, Guizhou, China;  
4. Department of Geosciences, College of Science, Virginia Tech, Blacksburg 24061, Virginia, USA; 5. The 271 Geological Team of  
the Guangxi Geology and Mineral Bureau, Guilin 541100, Guangxi, China; 6. Institute of Mineral Resources, Chinese Academy of  
Geological Sciences, Beijing 100037, China)

**Abstract:** This paper is the result of mineral exploration engineering.

**[Objective]** The Shuitoushan deposit is located in the south part of Baoshan block in the "Sanjiang" metallogenic belt, SW China. It is another important newly discovered epithermal Pb–Zn deposit in Zhenkang ore concentration area. Since no igneous rock exposed in the mining area, the origin of the ore deposit is still controversial. This paper aims to determine the genetic type of the deposit by studying on the sources of ore-forming materials and fluids. **[Methods]** Based on the detailed division of ore-forming stages of Shuitoushan deposit, the inductively coupled plasma mass spectrometer (ICP–MS) was used to systematically analyze rare earth elements of the rocks (ores) and sulfides in different stages. C and O isotopic compositions of the ore-hosted carbonate rocks, marbles and calcites of different stages were analyzed as well. Compared with the adjacent Luziyan super-large Pb–Zn–Fe polymetallic deposit, we discuss the sources of ore-forming materials and the characteristics of ore-forming fluids in the Shuitoushan deposit, and reveal the ore-forming mechanism of the deposit. **[Results]** The Shuitoushan deposit can be divided into mineralization stage and epigenetic stage. Among them, the mineralization stage can be further divided into stage I (pyrite–chalcocite–calcite stage), stage II (sphalerite–galena–calcite stage) and stage III (chalcocite–calcite stage). The studies of rare earth elements and C–O isotopic compositions show that the Y/Ho values of minerals and ores from each stage of Shuitoushan deposit indicate the source of the ore-forming materials is related to deep magmatic activity. Comparing the REE distribution model of minerals and ores from Shuitoushan deposit with the Yanshanian Kejie and Zhibenshan granites in the Baoshan block shows that the REEs in the ore-forming fluid of this deposit was mainly originated from deep magmatic hydrothermal fluid. As shown in the  $\delta^{13}\text{C}_{\text{V}-\text{PDB}}-\delta^{18}\text{O}_{\text{V}-\text{SMOW}}$  diagram, the ore-forming fluids are also mainly from magmatic hydrothermal fluids. During the migration processes, the ore-forming hydrothermal fluids was contaminated by sedimentary rocks in early stage, and may be affected by low-temperature alteration and atmospheric precipitation in later stages. **[Conclusions]** Both the sources of ore-forming materials and fluids of Shuitoushan deposit are closely related to the magmatic hydrothermal fluid in the deep part of the mining area. It has the same origin with the adjacent Luziyan super-large Pb–Zn–Fe polymetallic deposit, and is an epithermal deposit related to acidic magmatic hydrothermal fluids.

**Key words:** Pb–Zn deposit; rare earth elements; C–O isotopes; source of metallogenic materials; mineral exploration engineering; Shuitoushan; Baoshan block; Yunnan Province

**Highlights:** The characteristics of the ore-forming fluid and the sources of ore-forming materials of the Shuitoushan Pb–Zn deposit have been identified, which reveals that the Luziyan super large skarn Pb–Zn–Fe deposit and the surrounding shuitoushan epithermal Pb–Zn deposit in the Zhenkang ore concentration area of the Baoshan block have the same sources of the ore-forming fluids and materials. Both of them are the products of the same magmatic hydrothermal mineralization system. This achievement provides a scientific support for the study of regional mineral deposits and the summary of the mineralization laws of lead–zinc deposits.

**About the first author:** CHEN Yuhong, male, born in 1995, master, assistant engineer, engaged in mineral exploration and geological research of mineral deposits; E-mail: 630476104@qq.com.

**About the corresponding author:** ZHAO Jianxing, male, born in 1988, engineer, engaged in mineral exploration and geological research of mineral deposits; E-mail: 1770733128@qq.com.

**Fund support:** Supported by the National Natural Science Foundation of China (No.41363001, No.41762009).

## 1 引言

滇西保山地块位于滇缅泰马地块北缘,为西缅甸和印度支那地块的接触带(图1a),迄今已发现包括芦子园超大型矿床在内的近百个Pb-Zn-Fe-Cu多金属矿床(矿化点),是中国西南地区重要的Pb-Zn生产基地之一(邓明国等,2016)。在区内目前已知的大中型Pb-Zn矿床中,发育西邑、勐兴和东山等低温热液型(李志群等,2005;肖昌浩,2013;聂飞等,2015;陈福川,2018;刘锦康等,2020)以及芦子园、核桃坪和金厂河等矽卡岩型(陶琰等,2010;Yang et al., 2013;黄华等,2014;邓明国等,2016;Yang et al., 2016;Xu et al., 2019;刘学龙等,2022)2种最重要的Pb-Zn矿化类型(图1b)。水头山矿床是保山地块南段镇康Pb-Zn-Fe-Cu多金属矿集区内新近勘查发现的一个较为典型的低温热液型Pb-Zn矿床,与毗邻的芦子园超大型矽卡岩Pb-Zn-Fe-Cu多金属矿床仅6 km(图1c),其地质特征有别于保山地块内已知的2种Pb-Zn矿化类型,其产出部位、赋矿地层及中低温矿物共生组合(黄铜矿、雌黄铁矿和毒砂)和与岩浆热液有关的芦子园等矽卡岩型Pb-Zn-Fe-Cu矿床有相似之处,但围岩蚀变(普遍发育硅化、碳酸盐化、绿泥石化)未见矽卡岩化,其蚀变程度明显强于地块内的浅成低温热液矿床,而成矿流体、成矿物质来源以及形成机制是否与地块内的2种铅锌多金属矿化类型矿床一致?这是目前亟需解决的科学问题。前人仅对该矿床的地质特征进行过初步研究(陈明勇,2014;杨飞,2015;邓明国等,2017;张传昱等,2022),但其整体研究程度较低,尤其稀土元素和C-O同位素地球化学等方面的研究尚属空白,制约了对该矿床成矿物质来源的深入认识。

近年来,稀土元素地球化学在示踪Pb-Zn矿床成矿物质来源、成矿流体来源和反演成矿流体演化过程等方面,已得到了广泛应用(Li et al., 2007;Huang et al., 2010;周家喜等,2012);Pb-Zn矿床中热液碳酸盐矿物的C同位素是示踪碳质来源的有效

方法(毛景文等,2003;Huang et al., 2010;Zhou et al., 2013;丁伟品等,2022)。然而,由于成矿作用的复杂性,仅仅利用单一或少量的稀土元素或同位素数据可能会导致片面、甚至相互矛盾的结论(Kerrick et al., 2000)。因此,本文选取新近发现的水头山矿床喻空矿段主矿体作为研究对象,在详细的矿床地质特征研究的基础上,划分了该矿床的成矿期次和成矿阶段,通过系统采集水头山矿床成矿期不同阶段的典型代表性样品,开展了各阶段不同矿物的稀土元素及C-O同位素地球化学组成研究,并与毗邻的芦子园超大型矿床进行综合对比,探讨了水头山矿床成矿物质、成矿流体来源,揭示矿床的成矿机理。同时,对提升保山地块南部区域成矿规律的认识具有重要意义。

## 2 矿床地质概况

水头山Pb-Zn矿床位于腾冲地块与昌宁—孟连缝合带结合部西侧的保山地块南段镇康Pb-Zn-Fe-Cu多金属矿集区(图1b)。区内燕山晚期的志本山和柯街S型花岗岩是与地壳物质深熔作用有关的高钾过铝质花岗岩,被认为与保山地块内的芦子园和核桃坪Pb-Zn-Fe等多金属矿化有关(陶琰等,2010),但迄今为止,矿集区内已知矿床的深边部均尚未见到岩体,与保山地块内Pb-Zn矿化有关的成矿作用尚不明确。

水头山矿区出露地层主要为上寒武统沙河厂组( $\epsilon_s$ )和保山组( $\epsilon_b$ )碎屑岩、碳酸盐岩及大理岩,其中保山组第一段为水头山矿床的主要含矿地层(图2a)。矿区内褶皱和断裂发育,主要由乌木兰背斜和NW、NEE及近EW向的断裂构成。其中,NEE向组断裂具有张扭性质,控制着矿区内所有矿体的产出,与成矿作用关系紧密,为区内最主要的控矿构造;NW向组断裂则具张扭转压扭性质,为成矿后期的破矿构造。

水头山矿床受成岩后断裂控矿明显,矿体主要呈似层状、透镜状产出,具走向延伸长和厚度大的特点。初步查明隐伏工业矿体6个,且多赋存于

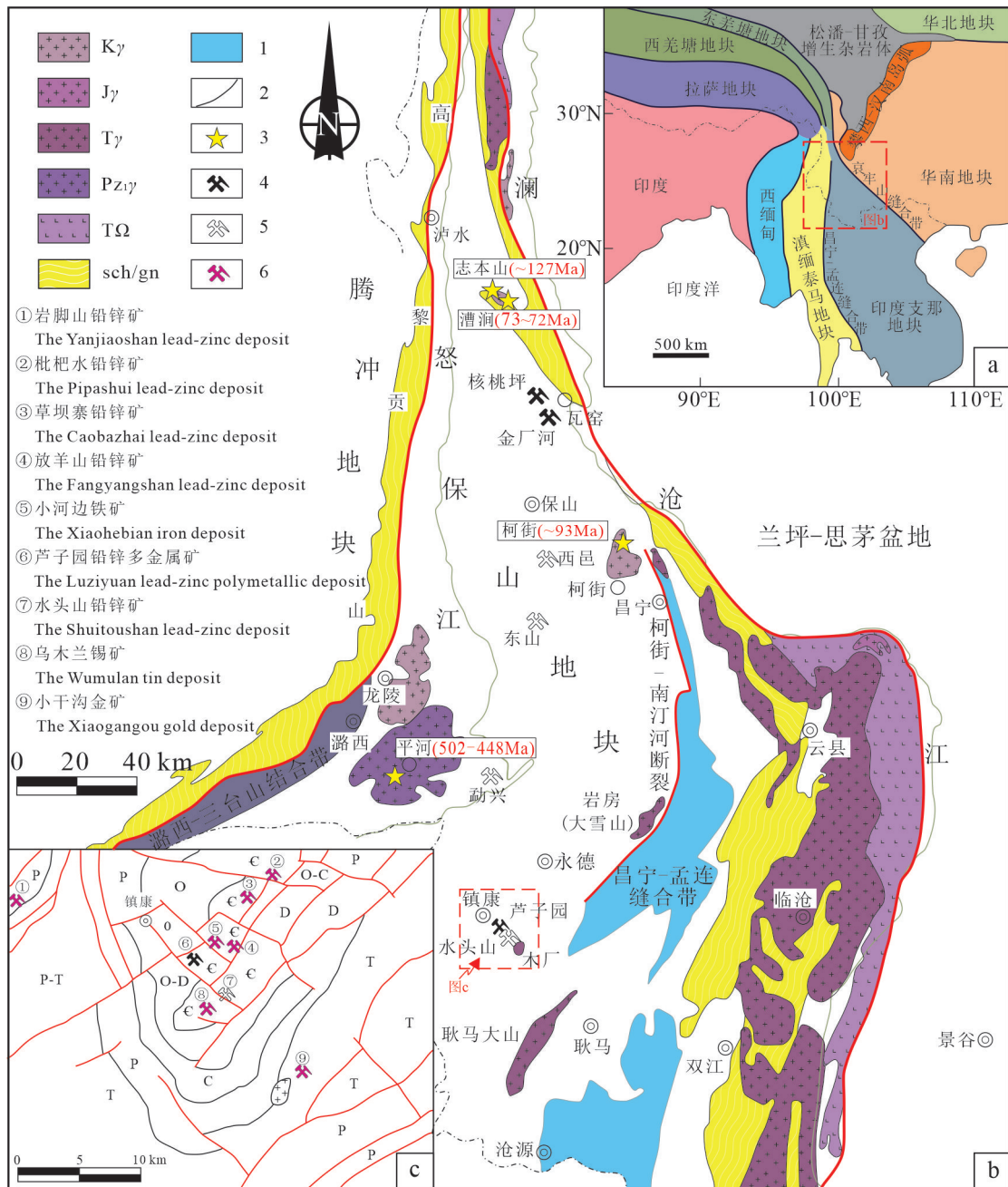


图1 西南三江地区构造示意图(a, 底图据 Metcalfe, 2013), 保山地块构造缝合带、花岗岩及矿床分布地质简图(b, 底图据 Deng et al., 2014a), 镇康矿集区矿产分布图(c, 据夏庆霖等, 2005)

K<sub>y</sub>—白垩纪花岗岩; J<sub>y</sub>—侏罗纪花岗岩; T<sub>y</sub>—三叠纪花岗岩; P<sub>z,y</sub>—早古生代花岗岩; TΩ—三叠纪火山岩; sch/gn—片岩/片麻岩; 1—含洋盆火山混杂岩; 2—构造边界断裂; 3—主要岩体及年龄; 4—矽卡岩型矿床; 5—低温热液型矿床; 6—热液多金属矿床; 志本山岩体与柯街岩体年龄引自陶琰等(2010); 曹洞岩体年龄引自廖世勇等(2013), 禹丽等(2014); 平河岩体年龄引自 Chen et al. (2007), Liu et al. (2009), Dong et al. (2013)

Fig.1 Schematic tectonic map of southeast Sanjiang region (a, after Metcalfe, 2013); simplified geological map of the Baoshan block, suture zones, granites and deposits (b, after Deng et al., 2014a); the mineral distribution map of Zhenkang Ore-Concentration area (c, after Xia Qinglin et al., 2005)

K<sub>y</sub>—Cretaceous granite; J<sub>y</sub>—Jurassic granite; T<sub>y</sub>—Triassic granite; P<sub>z,y</sub>—Early Paleozoic granite; TΩ—Triassic volcanic rock; sch/gn—schist/gneiss; 1—Oceanic volcanic melange; 2—Tectonic boundary fault; 3—Main rock mass and age; 4—Skarn deposit; 5—Low temperature hydrothermal deposit; 6—Hydrothermal polymetallic deposit; The ages of the Zhibenshan granite and Kejie granite are from Tao Yan et al. (2010); The ages of the Caojian granite are from Liao Shiyong et al. (2013) and Yu Li et al. (2014); The ages of the Pinghe granite are from Chen et al. (2007), Liu et al. (2009) and Dong et al. (2013)

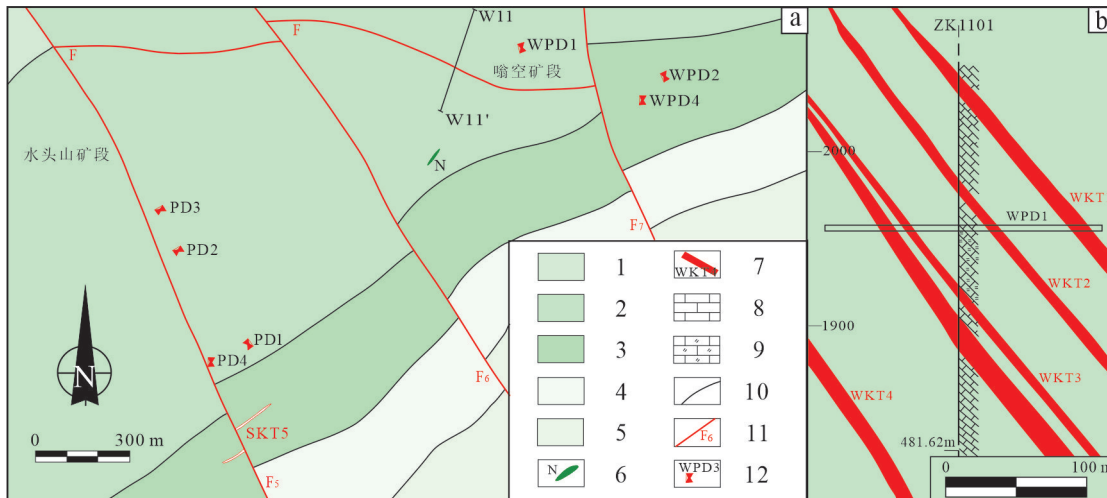


图2 水头山矿床地质简图(a),W11号勘探线剖面示意图(b)(据云南省地质调查院修编,2016<sup>①</sup>)

1—上寒武统保山组第二段;2—上寒武统保山组第一段二亚段;3—上寒武统保山组第一段一亚段;4—上寒武统沙河厂组第三段二亚段;5—上寒武统沙河厂组第三段一亚段;6—基性岩脉;7—Pb-Zn 矿体及编号;8—灰岩;9—白云质灰岩;10—实测地质界线;11—实测断层及编号;12—平硐位置及编号

Fig.2 Simplified geological map of the Shuitoushan Pb-Zn deposit (a); Geological section map along W-No.11 exploration line (b)  
(modified from the Yunnan Geological Survey, 2016<sup>①</sup>)

1—The second member of Baoshan Formation of Upper Cambrian; 2—The second sub-member of the first member of Baoshan Formation of Upper Cambrian; 3—The first sub-member of the first member of Baoshan Formation of Upper Cambrian; 4—The second sub-member of the third member of Shahechang Formation of Upper Cambrian; 5—The first sub-member of the third member of Shahechang Formation of Upper Cambrian; 6—Mafic dikes; 7—Lead-zinc ore body and number; 8—Limestone; 9—Dolomitic limestone; 10—Practical survey of geological boundary; 11—Measured fault and number; 12—Adit location and number

2050 m 标高以下的大理岩化灰岩构造破碎带中。其按空间分布特征分为水头山和嗡空两个矿段,其中嗡空矿段资源储量占绝对优势,目前已探明主矿体4个(WKT1、WKT2、WKT3 和 WKT4),其勘查程度较高,为本文主要研究对象(图2b)。

矿床由浅到深,矿石出现氧化矿→混合矿→原生矿的规律性变化。矿石中普遍发育块状(图3c)、稀疏浸染脉状(图3b)、网脉-浸染状、稠密浸染状构造(图3a),偶见斑杂状、网脉状(图3d)和角砾状构造;矿石结构主要为他形—半自形粒状结构、共生边结构、压碎结构(图3f)、变晶结构、筛孔-骸晶结构、溶蚀-残余结构(图3e)、交代脉状结构(图3e,g,h)和交代网状结构等;围岩蚀变有方解石化、白云石化、绿泥石化、硅化和绢云母化等中低温热液蚀变特点。

根据野外调查和室内岩矿显微鉴定,将该矿床成矿期次划分为热液成矿期和表生期。热液成矿期又可划分为3个成矿阶段,由早到晚依次为阶段I(黄铁矿-黄铜矿-方解石阶段)、阶段II(闪锌矿-方铅矿-方解石主成矿阶段)和阶段III(黄铜

矿-方解石阶段)(表1)。阶段I与芦子园热液成矿期早硫化物阶段相对应(邓明国等,2016),形成黄铁矿、黄铜矿、毒砂、白铁矿、白云石、绢云母、石英、绿泥石及方解石等矿物组合,其中黄铁矿形成较早,具同心环状、压碎结构,且多沿围岩的裂隙呈星点状、网脉状及浸染状分布于胶结物及角砾中,而黄铜矿则普遍以交代方式包围、穿插黄铁矿(图3c~f);阶段II为闪锌矿和方铅矿产出的主要阶段,与芦子园矿床热液成矿期晚硫化物阶段相对应(邓明国等,2016),白云石、石英、绿泥石和方解石大量产出,偶见磁黄铁矿和白铁矿,其中闪锌矿具多种颜色,为他形粒状结构,多沿围岩裂隙呈脉状产出,而方铅矿除部分呈他形粒状分布于围岩的裂隙中外,多沿闪锌矿的边缘及其粒间穿插交代,可见其与闪锌矿形成共生边结构,同时或分别沿黄铜矿、黄铁矿的粒间裂隙呈尖角状交代(图3a,b,d,g);阶段III主要以早阶段形成的矿体被无矿石英脉和方解石脉切穿为特征,亦可见黄铜矿呈不规则状穿插,包围交代闪锌矿和方铅矿的现象,代表了热液

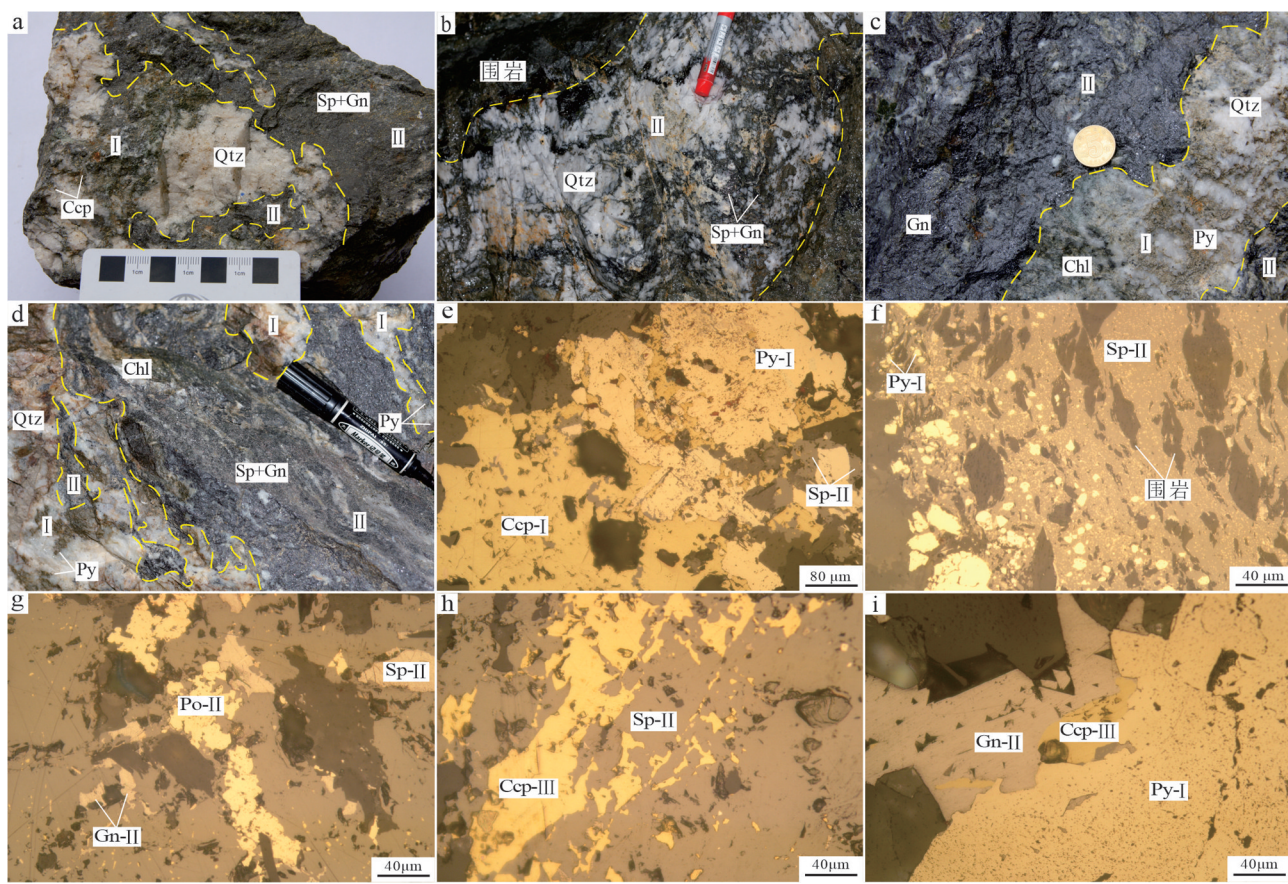


图3 水头山矿床矿石结构特征

a—稠密浸染状铅锌铜矿石;b—稀疏浸染状铅锌矿石;c—块状方铅矿矿石;d—稠密浸染状、脉状铅锌矿石;e—黄铜矿—I穿插交代黄铁矿—I,闪锌矿-II则呈脉状分布;f—闪锌矿-II沿围岩裂隙呈脉状产出;g—一方铅矿-II、磁黄铁矿-II穿插交代闪锌矿-II;h—黄铜矿-III穿插交代闪锌矿-II;i—黄铜矿-III穿插交代方铅矿-II;I—阶段I;II—阶段II;III—阶段III;Py—黄铁矿;Ccp—黄铜矿;Sp—闪锌矿;Gn—一方铅矿;Po—磁黄铁矿;Chl—绿泥石;Qtz—石英

Fig.3 Petrofabric characteristics of the Shuitoushan Pb-Zn ores

a—Dense disseminated lead zinc copper ore; b—Sparsely disseminated lead-zinc ores; c—Massive galena ore; d—Dense disseminated, veined lead-zinc ore; e—Chalcopyrite—I interspersed with metasomatic pyrite—I, sphalerite—II distributed in vein; f—Sphalerite—II produced in vein along the fissure of surrounding rock; g—Galenite—II, magenta—II ore interpolated for sphalerite—II; h—Chalcopyrite—III intercalation with metasomatic sphalerite—II; i—Chalcopyrite—III interspersed with metasomatic galena—II; I—Stage I; II—Stage II; III—Stage III; Py—Pyrite; Ccp—Chalcopyrite; Sp—Sphalerite; Gn—Galena; Po—Pyrrhotite; Chl—Chlorite; Qtz—Quartz

成矿作用的结束(图3h,i)。表生期形成的矿物主要为褐铁矿、孔雀石、菱锌矿和白铅矿等。

### 3 样品采集与分析方法

本次研究样品采自水头山矿床喻空矿段方解石及石英分布广泛的1820、1930、1956中段的主成矿期矿体,主要针对碳酸盐岩、大理岩、矿石及与金属矿物共生的方解石分别进行采样,选取其中具有代表性的新鲜岩(矿)石样品挑选单矿物,用作稀土元素及C-O同位素分析。其中稀土元素分析为水头山矿床阶段I(黄铜矿、黄铁矿)、阶段II(闪锌

矿、方铅矿和方解石)、阶段III(黄铜矿)以及矿石、围岩、芦子园矿床早硫化物阶段(方解石)和晚硫化物阶段(方铅矿、黄铜矿和方解石)样品;C-O同位素样品为阶段II与闪锌矿和方铅矿密切共生的热液方解石及阶段III与黄铜矿共生的方解石脉。将岩(矿)石样品在玛瑙研钵中手工逐级破碎,过筛至40~60目,经淘洗、低温烘干后在双目显微镜下重复多次挑选,以确保样品纯度优于99%。

(1)稀土元素分析:岩(矿)石及单矿物稀土元素测试由核工业北京地质研究院和中国科学技术大学地球与空间科学学院固体同位素地球化学实

验室共同完成。挑纯后的样品均用陶瓷研钵研磨至200目,首先准确称取15 mg样品置于10 m Teflon六角瓶中,再加入0.5 mL HCl,1 mL HNO<sub>3</sub>,拧紧瓶盖后放入烤箱中,在105℃加热24 h,然后打开瓶盖并定容至15 mL待测。采用电感耦合等离子体质谱仪(ICP-MS)进行稀土元素定量测试,采取的测试方法和依据为《硅酸盐岩石化学分析方法第30部分:44个元素量测定》(GB/T14506.30-2010),测试温度为20℃,相对湿度为30%。分析误差一般小于10%。

(2)C-O同位素分析:碳酸盐岩、大理岩及方解石C-O同位素测试在核工业北京地质研究院完成。将挑纯后的样品在陶瓷研钵中研磨成200目,用电子天平称取0.1 g放于烘箱中烘干,然后在真空系统中于25℃下与100%的正磷酸反应24 h。生成的CO<sub>2</sub>气体进入IRMS(Isoprime)质谱仪进行测试C-O同位素组成。分析结果用PDB结果表示,精度为0.2‰,具体分析方法见向世红等(2013)。

## 4 分析结果

### 4.1 稀土元素特征

水头山矿床矿石矿物(闪锌矿、方铅矿、黄铜矿、黄铁矿)、脉石矿物(方解石)、矿石(碳酸盐岩型

矿石)、围岩(碳酸盐岩)与区域花岗岩(柯街、志本山)稀土元素含量及特征参数见表2,与Taylor and McLennan(1985)球粒陨石相比的稀土元素配分曲线图详见图4和图5。

水头山矿床矿石矿物的稀土元素特征,阶段Ⅱ闪锌矿ΣREE含量相对较低,3件不同颜色闪锌矿样品的ΣREE含量为0.4×10<sup>-6</sup>~1.157×10<sup>-6</sup>,均值为0.655×10<sup>-6</sup>;ΣLREE/ΣHREE为1.837~5.322,均值为3.496,具有相对富集轻稀土的特点;δEu为0.616~1.656,具有弱的负铕异常到弱的正铕异常特征,均值为1.188,总体表现为弱的正铕异常;δCe为0.842~0.942,均值为0.893,显示弱的负铈异常特征(图4a);阶段Ⅱ方铅矿ΣREE含量普遍较低,2件方铅矿样品的ΣREE含量为0.249×10<sup>-6</sup>~0.88×10<sup>-6</sup>,均值为0.565×10<sup>-6</sup>;ΣLREE/ΣHREE为0.504~5.385,均值为2.945,表现为相对富集轻稀土的特点;δEu为0.370~1.201,均值为0.786,为弱的负铕异常;δCe为0.681~0.737,均值为0.709,具有弱的负铈异常特征(图4c);阶段Ⅰ黄铜矿ΣREE含量为2.004×10<sup>-6</sup>,ΣLREE/ΣHREE为9.547,δEu为0.241,明显为负铕异常,δCe为0.943,铈负异常弱;阶段Ⅰ黄铁矿ΣREE含量为1.011×10<sup>-6</sup>,ΣLREE/ΣHREE为

表1 水头山矿床矿物生成顺序表

Table 1 The mineral arisen sequence of the Shuitoushan Pb-Zn deposit

矿物	热液成矿期			表生期
	黄铁矿-黄铜矿 -方解石阶段(I)	闪锌矿-方铅矿 -方解石阶段(II)	黄铜矿-方解 石阶段(III)	
白云石				
黄铁矿	●			
白钛矿	●			
毒砂	●			
绢云母	●			
黄铜矿	●		●	
石英	●		●	
绿泥石	●			
方解石	●		●	
闪锌矿		●		
方铅矿		●		
磁黄铁矿		●		
白铁矿		●		
褐铁矿		●		
孔雀石		●		
菱锌矿		●		
白铅矿		●		

表2 水头山矿床及芦子园矿床稀土元素含量( $10^{-6}$ )及特征参数  
Table 2 REE content ( $10^{-6}$ ) and characteristics parameter of the Shuitoushan Pb-Zn deposit and Luyiyuan Pb-Zn-Fe polymetallic deposit

名称	样品号	测试对象	成矿阶段	$\delta\text{Eu} = \frac{\text{Eu}_{\text{样品}} - \text{Eu}_{\text{标准陨石}}}{\text{Eu}_{\text{标准陨石}}} \times 10^4$														$\sum \text{LREE}/\sum \text{HREE}$	$\delta\text{Eu}$	$\delta\text{Ce}$
				La	Ce	Pr	Nd	Sm	Eu	Gd	Tb	Dy	Ho	Er	Tm	Yb	Lu	Y		
No.2	浅棕色浸染 状闪锌矿 <sup>a</sup>	阶段II	0.070 0.113 0.013 0.048 0.010 0.005 0.008 0.002 0.008 0.002 0.002 0.007 0.004 0.002 0.002 0.106 0.400 0.259 0.141 1.837 1.656 0.842																	
	深棕色稠密 浸染状 闪锌矿 <sup>a</sup>	阶段II	0.228 0.439 0.051 0.209 0.040 0.007 0.027 0.005 0.020 0.003 0.006 0.002 0.008 0.002 0.110 1.157 0.974 0.183 5.322 0.616 0.942																	
No.8	浅棕色细脉 状闪锌矿 <sup>a</sup>	阶段II	0.071 0.139 0.019 0.066 0.013 0.005 0.01 0.002 0.008 0.002 0.004 0.002 0.005 0.002 0.002 0.059 0.407 0.313 0.094 3.330 1.292 0.894																	
	No.10	方铅矿 <sup>a</sup>	阶段II	0.069 0.098 0.013 0.074 0.037 0.004 0.027 0.010 0.030 0.013 0.032 0.006 0.013 0.002 0.412 0.880 0.295 0.585 0.504 0.370 0.737																
水头山 Pb-Zn 矿床	No.14	方铅矿 <sup>a</sup>	阶段II	0.074 0.086 0.009 0.027 0.011 0.003 0.002 0.004 0.002 0.005 0.002 0.002 0.002 0.017 0.249 0.210 0.039 5.385 1.201 0.681																
	No.3	黄铜矿 <sup>a</sup>	阶段I	0.404 0.812 0.101 0.402 0.089 0.006 0.057 0.009 0.027 0.004 0.008 0.002 0.006 0.002 0.075 2.004 1.814 0.190 9.547 0.241 0.943																
No.6	黄铜矿 <sup>a</sup>	阶段III	0.077 0.155 0.02 0.09 0.027 0.004 0.027 0.007 0.043 0.007 0.020 0.002 0.012 0.002 0.146 0.639 0.373 0.266 1.402 0.448 0.930																	
	No.3	黄铁矿 <sup>a</sup>	阶段I	0.091 0.198 0.031 0.121 0.043 0.007 0.047 0.011 0.054 0.012 0.032 0.005 0.026 0.005 0.328 1.011 0.491 0.520 0.944 0.474 0.895																
No.25	方解石	阶段II	16.8 31.9 3.96 15.3 3.37 2.01 3.38 0.72 4.2 0.862 2.28 0.379 2.17 0.259 31.6 119.19 73.34 45.85 1.600 1.803 0.911																	
	No.26	方解石	阶段II	7.82 11.3 1.31 5.21 1.3 0.887 1.7 0.382 2.63 0.578 1.57 0.277 1.59 0.215 23.2 59.969 27.827 32.142 0.866 1.824 0.778																
No.23	围岩	/	12.1 25.9 3.02 11.9 2.59 0.49 2.62 0.48 3.09 0.66 1.88 0.28 1.80 0.26 11.1 78.17 56 22.17 2.526 0.570 1.005																	
No.24	围岩	/	29.4 59.5 6.44 23.0 3.90 0.74 3.07 0.44 2.50 0.55 1.63 0.25 1.59 0.24 10.8 144.05 122.98 21.07 5.837 0.632 0.998																	
No.2	矽石	/	0.732 1.64 0.162 0.645 0.129 0.046 0.112 0.019 0.105 0.022 0.06 0.010 0.063 0.009 0.730 4.484 3.354 1.13 2.968 1.144 1.100																	
No.6	矽石 <sup>a</sup>	/	1.34 2.6 0.316 1.35 0.33 0.071 0.299 0.061 0.312 0.060 0.164 0.028 0.173 0.026 1.85 8.98 6.007 2.973 2.021 0.679 0.931																	
L19	闪锌矿 <sup>a</sup>	晚硫化物阶段	0.14 0.14 0.02 0.06 0.01 0 0.01 0 0.01 0 0 0 0 0 0 0 0.44 0.37 0.07 5.286 0.75 0.56																	
L26	闪锌矿 <sup>a</sup>	晚硫化物阶段	0.46 0.70 0.06 0.18 0.02 0 0.02 0 0.01 0 0 0 0 0 0 0 0.44 1.42 1.42 0.05 28.40 0.73 0.88																	
L8-5	闪锌矿 <sup>a</sup>	晚硫化物阶段	1.89 4.37 0.51 1.86 0.37 0.05 0.41 0.08 0.47 0.10 0.29 0.04 0.24 0.04 2.47 13.19 9.05 4.14 2.19 0.39 1.05																	
L15	闪锌矿 <sup>a</sup>	晚硫化物阶段	0.25 0.50 0.05 0.19 0.03 0 0.03 0.01 0.02 0 0.01 0 0.01 0 0.09 1.19 1.02 0.17 6.00 0.42 1.02																	
L41	方铅矿 <sup>a</sup>	晚硫化物阶段	0.031 0.036 0.005 0.016 0.009 0.002 0.005 0.002 0.002 0.002 0.002 0.002 0.002 0.002 0.018 0.136 0.099 0.037 2.676 0.831 0.632																	
L43	方铅矿 <sup>a</sup>	晚硫化物阶段	0.037 0.043 0.007 0.021 0.009 0.002 0.005 0.002 0.002 0.002 0.002 0.002 0.002 0.002 0.002 0.018 0.159 0.119 0.04 2.975 0.831 0.602																	
L44	黄铜矿 <sup>a</sup>	晚硫化物阶段	0.011 0.019 0.002 0.011 0.004 0.002 0.002 0.003 0.002 0.002 0.002 0.002 0.002 0.002 0.007 0.073 0.049 0.024 2.042 1.927 0.907																	
L45	黄铜矿 <sup>a</sup>	晚硫化物阶段	0.035 0.029 0.005 0.014 0.005 0.002 0.002 0.002 0.002 0.002 0.002 0.002 0.002 0.002 0.018 0.124 0.09 0.034 2.647 1.631 0.466																	
L47	方解石	晚硫化物阶段	6.44 14.2 1.78 1.84 0.767 1.76 0.365 2.08 0.397 1.04 0.183 1.07 0.13 13 52.482 32.457 20.025 1.621 1.286 0.994																	
L48	方解石	早硫化物阶段	1.61 5.76 1.08 6.55 1.97 0.214 1.01 0.107 0.361 0.051 0.127 0.015 0.096 0.012 1.95 20.913 17.184 3.729 4.608 0.416 1.015																	
KJ	区域花岗岩	/	52.1 105.0 11.2 37.7 7.33 0.76 5.51 1.05 6.04 1.27 3.67 0.54 3.83 0.55 34.9 271.45 214.09 57.36 3.732 0.351 1.00																	
ZBS	区域花岗岩	/	24.7 50.1 5.56 20.4 4.54 1.11 3.59 0.65 3.88 0.81 2.28 0.34 2.29 0.34 24.0 144.59 106.41 38.18 2.787 0.813 0.99																	

注:球粒陨石标准化数据引自 Taylor and McLennan, 1985;  $\delta\text{Eu} = 2(\text{Eu}_{\text{样品}}/\text{Eu}_{\text{标准陨石}})/(\text{Sm}_{\text{样品}}/\text{Sm}_{\text{标准陨石}} + \text{Gd}_{\text{样品}}/\text{Gd}_{\text{标准陨石}})$ ;  $\delta\text{Ce} = 2(\text{Ce}_{\text{样品}}/\text{Ce}_{\text{标准陨石}})/(\text{La}_{\text{样品}}/\text{La}_{\text{标准陨石}} + \text{Pr}_{\text{样品}}/\text{Pr}_{\text{标准陨石}})$ ; 壬子园矿床4个闪锌矿<sup>a</sup>样品L19、L26、L8-5及L15均引自邓明国等, 2016; 保山地块2个区域花岗岩样品KJ(柯街)、ZBS(志本山)均引自陶琰等, 2010。

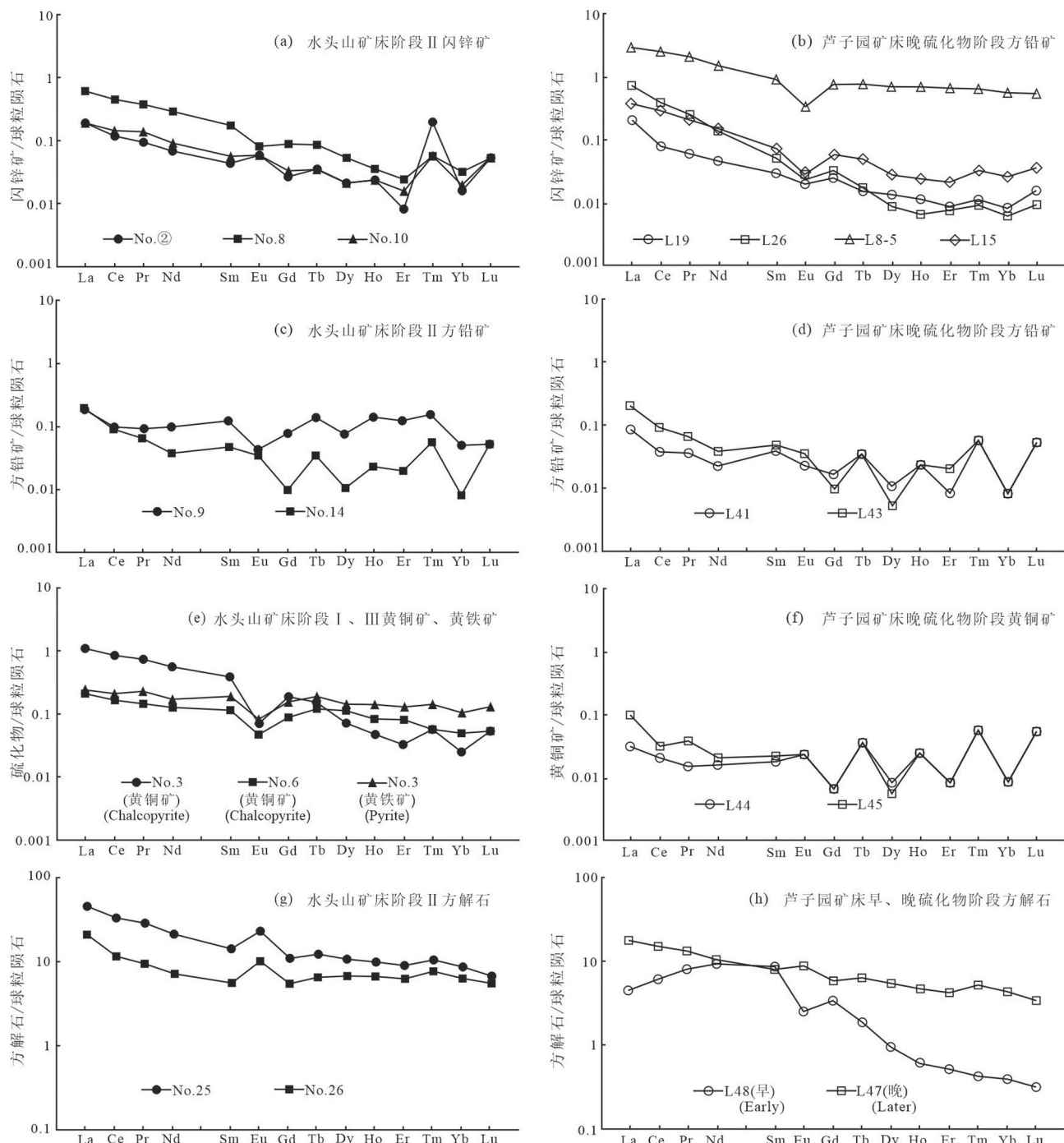


图4 水头山矿床及芦子园矿床单矿物稀土元素球粒陨石配分曲线

a—水头山矿床阶段Ⅱ闪锌矿;b—芦子园矿床晚硫化物阶段闪锌矿;c—水头山矿床阶段Ⅱ方铅矿;d—芦子园矿床晚硫化物阶段方铅矿;e—水头山阶段Ⅰ、Ⅲ黄铜矿、黄铁矿;f—芦子园矿床晚硫化物阶段黄铜矿;g—水头山矿床阶段Ⅱ方解石;h—芦子园矿床早、晚硫化物阶段方解石;球粒陨石标准化数据引自Taylor and McLennan, 1985

Fig.4 Chondrite-normalized REE patterns of the single mineral separates of Shuitoushan and Luziyuan deposit  
 a-The Ⅱ stage of sphalerite in the Shuitoushan deposit; b-The late sulfide stage of sphalerite in the Luziyuan deposit; c-The Ⅱ stage of galena in the Shuitoushan deposit; d-The late sulfide stage of galena in the Luziyuan deposit; e-The I, Ⅲ stage of chalcopyrite and pyrite in the Shuitoushan deposit; f-The late sulfide stage of chalcopyrite in the Luziyuan deposit; g-The Ⅱ stage of calcite in the Shuitoushan deposit; h-The early and late sulfide stages of calcite in the luziyuan deposit); REE chondrite-normalized after Taylor and McLennan, 1985

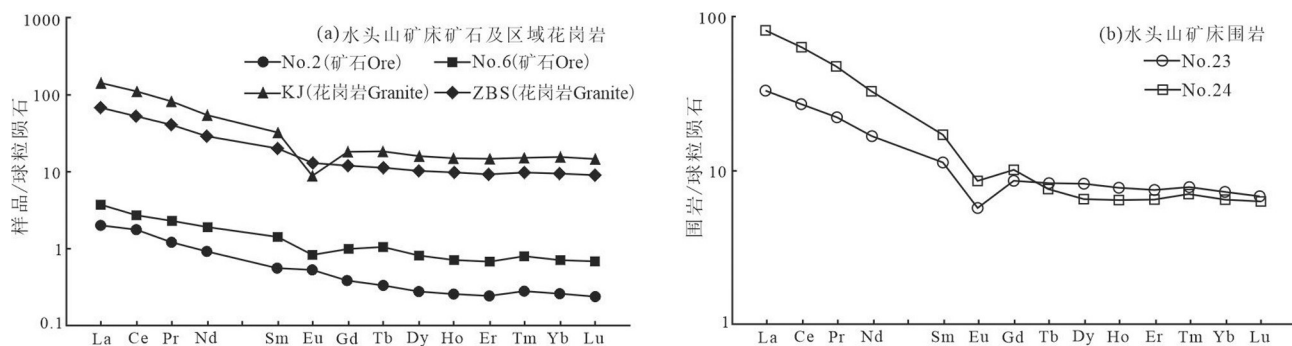


图5 水头山矿床矿石、围岩及区域花岗岩稀土元素球粒陨石配分曲线

a—水头山矿床矿石及区域花岗岩;b—水头山矿床围岩;球粒陨石标准化数据引自 Taylor and McLennan, 1985;保山地块柯街、志本山花岗岩数据引自陶琰等, 2010

Fig.5 Chondrite-normalized REE patterns of the ore and wallrock separates of Shuitoushan deposit and the area of granite  
a—The main mineralization stage of ore in the Shuitoushan deposit and regional granite; b—The surrounding rock in the Shuitoushan deposit; REE chondrite-normalized after Taylor and McLennan, 1985; The data of the Kejie and Zhibenshan granite of the Baoshan Block are after Tao Yan et al., 2010

0.944,  $\delta_{\text{Eu}}$  为 0.474, 为负铕异常;  $\delta_{\text{Ce}}$  为 0.895, 为弱的负铈异常; 阶段Ⅲ黄铜矿  $\Sigma \text{REE}$  含量为  $0.639 \times 10^{-6}$ ,  $\Sigma \text{LREE}/\Sigma \text{HREE}$  为 1.402,  $\delta_{\text{Eu}}$  为 0.448, 表现为负铕异常,  $\delta_{\text{Ce}}$  为 0.930, 亦为弱铈负异常(图4e)。

水头山矿床脉石矿物的稀土特征,阶段Ⅱ方解石  $\Sigma \text{REE}$  含量较高,2件方解石样品的  $\Sigma \text{REE}$  含量为  $59.969 \times 10^{-6} \sim 119.19 \times 10^{-6}$ , 均值为  $89.580 \times 10^{-6}$ ;  $\Sigma \text{LREE}/\Sigma \text{HREE}$  为 0.866~1.600, 均值为 1.233, 轻稀土与重稀土分馏程度较低;  $\delta_{\text{Eu}}$  为 1.803~1.824, 均值为 1.814, 正铕异常明显;  $\delta_{\text{Ce}}$  为 0.778~0.911, 均值为 0.845, 为弱的负铈异常特征(图4g)。

水头山矿床矿石的稀土特征,碳酸盐岩型矿石  $\Sigma \text{REE}$  含量相对金属硫化物(图4)较高,2件矿石样品的  $\Sigma \text{REE}$  含量为  $4.484 \times 10^{-6} \sim 8.98 \times 10^{-6}$ , 均值为  $6.732 \times 10^{-6}$ ;  $\Sigma \text{LREE}/\Sigma \text{HREE}$  为 2.021~2.968, 均值为 2.495, 轻稀土与重稀土分异明显;  $\delta_{\text{Eu}}$  为 0.679~1.144, 均值为 0.912, 表现为弱的负铕异常;  $\delta_{\text{Ce}}$  为 0.931~1.100, 均值为 1.016, 正铈异常较为微弱(图5a)。

水头山矿床的围岩为碳酸盐岩,其  $\Sigma \text{REE}$  含量较高,2件围岩样品的  $\Sigma \text{REE}$  为  $78.17 \times 10^{-6} \sim 144.05 \times 10^{-6}$ , 均值为  $111.11 \times 10^{-6}$ ;  $\Sigma \text{LREE}/\Sigma \text{HREE}$  为 2.526~5.837, 均值为 4.182, 轻重稀土明显分异;  $\delta_{\text{Eu}}$  为 0.570~0.632, 均值为 0.601, 为负铕异常;  $\delta_{\text{Ce}}$  为 0.998~1.005, 均值为 1.002, 铈异常不明显(图5b)。

#### 4.2 C-O同位素特征

由于C-O同位素在不同地球化学端元间易分

馏,因而常被用来示踪成矿物质来源(袁波等, 2014)。本文选取了矿区内的围岩碳酸盐岩(偶见大理岩),以及与矿化关系密切的脉石矿物方解石为研究对象,对其进行C-O同位素测定以示踪该矿床碳源,分析结果见表3。

矿床脉石矿物的分析数据表明,不同阶段的热液方解石具有明显不同的  $\delta^{13}\text{C}_{\text{V}-\text{PDB}}$  和  $\delta^{18}\text{O}_{\text{V}-\text{SMOW}}$  值。2件阶段Ⅰ方解石,  $\delta^{13}\text{C}_{\text{V}-\text{PDB}}$  值为  $-7.78\text{\textperthousand} \sim -6.59\text{\textperthousand}$ , 均值为  $-7.185\text{\textperthousand}$ ,  $\delta^{18}\text{O}_{\text{V}-\text{SMOW}}$  值为  $7.59\text{\textperthousand} \sim 8.14\text{\textperthousand}$ , 均值为  $7.865\text{\textperthousand}$ ; 2件阶段Ⅱ方解石C、O同位素组成相对均一,其  $\delta^{13}\text{C}_{\text{V}-\text{PDB}}$  值为  $-0.6\text{\textperthousand} \sim 0.5\text{\textperthousand}$ , 均值为  $-0.05\text{\textperthousand}$ ,  $\delta^{18}\text{O}_{\text{V}-\text{SMOW}}$  值为  $11.4\text{\textperthousand} \sim 12\text{\textperthousand}$ , 均值为  $11.7\text{\textperthousand}$ ; 2件阶段Ⅲ方解石  $\delta^{13}\text{C}_{\text{V}-\text{PDB}}$  值为  $-6.5\text{\textperthousand} \sim -5\text{\textperthousand}$ , 均值为  $-5.75\text{\textperthousand}$ ,  $\delta^{18}\text{O}_{\text{V}-\text{SMOW}}$  值为  $9.8\text{\textperthousand} \sim 10.5\text{\textperthousand}$ , 均值为  $10.15\text{\textperthousand}$ 。

矿区围岩的  $\delta^{13}\text{C}_{\text{V}-\text{PDB}}$  值和  $\delta^{18}\text{O}_{\text{V}-\text{SMOW}}$  值与阶段Ⅲ方解石的相近,大理岩的  $\delta^{13}\text{C}_{\text{V}-\text{PDB}}$  值为  $-7.5\text{\textperthousand}$ ,  $\delta^{18}\text{O}_{\text{V}-\text{SMOW}}$  值为  $12.2\text{\textperthousand}$ ; 碳酸盐岩的  $\delta^{13}\text{C}_{\text{V}-\text{PDB}}$  值为  $-5.5\text{\textperthousand}$ ,  $\delta^{18}\text{O}_{\text{V}-\text{SMOW}}$  值为  $10.8\text{\textperthousand}$ 。

## 5 讨论

### 5.1 成矿物质来源

稀土元素在参与地质演化过程中具有相近的地球化学行为与特征(王中刚等, 1989; 庞绪成等, 2010; 龙汉生等, 2011),是一种示踪矿床形成环境的有用指标(Lottermoser, 1989)。由球粒陨石标准

表3 水头山矿床C–O同位素组成  
Table 3 C and O isotopic compositions of the Shuitoushan Pb–Zn deposit

样品号	采样位置/m	测试对象	成矿阶段	$\delta^{13}\text{C}_{\text{V-PDB}}/\text{\textperthousand}$	$\delta^{18}\text{O}_{\text{V-PDB}}/\text{\textperthousand}$	$\delta^{18}\text{O}_{\text{V-SMOW}}/\text{\textperthousand}$
No.20	WPD1-1956	方解石	阶段 I	-6.59	-22.57	7.59
No.20	WPD1-1956	方解石	阶段 I	-7.78	-22.04	8.14
No.20	WPD1XJ-1930	方解石	阶段 II	0.5	-18.3	12
No.21	WPD2-1820	方解石	阶段 II	-0.6	-18.9	11.4
No.18	WPD1-1956	方解石	阶段 III	-5	-19.8	10.5
No.19	WPD1-1956	方解石	阶段 III	-6.5	-20.5	9.8
No.22	WPD1-1956	大理岩	/	-7.5	-18.2	12.2
No.23	WPD2-1820	碳酸盐岩	/	-5.5	-19.5	10.8

注:  $\delta^{18}\text{O}_{\text{V-SMOW}}(\text{\textperthousand})$  值计算根据平衡方程  $\delta^{18}\text{O}_{\text{V-SMOW}} = 1.03086 \delta^{18}\text{O}_{\text{V-PDB}} + 30.86$  (Friedman and O'Neil, 1977)。

化稀土元素配分模式可知,水头山矿床金属矿物阶段Ⅱ不同颜色闪锌矿,抑或阶段Ⅱ不同硫化物间稀土元素配分模式(图4a、c)极为相似,及各阶段不同硫化物间稀土元素配分模式(图4a、c、e)相近,并与芦子园矿床各阶段不同硫化物间稀土元素配分模式(图4b、d、f)基本吻合,暗示在沉淀金属硫化物时,成矿流体中的REE组成及物化条件未发生显著变化,因而可以用该矿床各阶段金属硫化物的稀土元素来示踪成矿流体的来源(Henderson, 1984;周家喜等,2010;王立强等,2012)。

水头山矿床硫化物极为发育,主要为闪锌矿,次为方铅矿,偶见黄铜矿和黄铁矿,暗示成矿流体中含有大量高活性S<sup>2-</sup>,暗示成矿流体的还原环境(周家喜等,2010,2012)。同时该矿床各阶段硫化物ΣREE含量( $0.249 \times 10^{-6} \sim 2.004 \times 10^{-6}$ )普遍较低,ΣLREE/ΣHREE值(0.504~9.547)相对较高,但阶段I( $\delta\text{Eu}=0.241 \sim 0.474$ )和阶段III( $\delta\text{Eu}=0.448$ )硫化物明显亏损Eu,而阶段II硫化物具负Eu异常到正Eu异常特征( $\delta\text{Eu}=0.370 \sim 1.656$ ),总体为弱的正Eu异常( $\delta\text{Eu}$ 均值为1.027)。由稀土元素的氧化还原模式可知(Chen and Zhao, 1997),水头山矿床硫化物形成于成矿流体的缺氧还原环境,其Eu应该富集而不应该为负异常,且碳酸盐岩地层不可能淋滤出富含REE的流体(Michard, 1989),表明引起该矿床各阶段硫化物中出现Eu负异常的可能原因:一是成矿流体中REE来源亏损Eu,二是各阶段与硫化物共生的方解石富集Eu。前已述及,该矿床最主要的脉石矿物为方解石,其他脉石矿物含量相对较少,阶段II与硫化物共生的方解石具明显的正Eu异常,且阶段II硫化物中也出现正Eu异常,显然可以排除第

二种可能,因此认为该矿床成矿流体中REE来源本身是亏损Eu的,但各阶段硫化物形成环境仍为缺氧还原环境。

水头山矿床矿石矿物、脉石矿物样品的轻稀土相对富集,ΣLREE/ΣHREE基本大于1,δCe均小于1,不同阶段矿石矿物、脉石矿物的稀土元素配分模式大体一致,均为右倾型(图4a、c、e、g),说明不同阶段单矿物具有相同的稀土来源,为同源不同阶段的产物,这与野外地质观察而划分的不同成矿阶段相吻合。此外,水头山矿床矿石、围岩及区域花岗岩具有轻稀土相对富集右倾型的稀土元素特征(图5)。ΣREE、ΣLREE均表现为矿石(前者为 $6.732 \times 10^{-6}$ ;后者为 $4.681 \times 10^{-6}$ )<围岩(前者为 $111.11 \times 10^{-6}$ ;后者为 $89.49 \times 10^{-6}$ )<花岗岩(前者为 $208.02 \times 10^{-6}$ ;后者为 $160.25 \times 10^{-6}$ )的变化特征,且矿石的稀土元素配分曲线特征与花岗岩的更为相似,这在很大程度上反映了该矿床的形成与花岗岩之间的成因联系。结合矿床地质背景,进一步确认该矿床的成矿物质来源与深部岩浆热液有关。

水头山矿床矿石矿物(闪锌矿、方铅矿、黄铜矿、黄铁矿)、脉石矿物(方解石)及矿石(碳酸盐岩型矿石)与区域花岗岩(志本山、柯街)的稀土元素配分模式十分相近(图4、图5),亦分别与芦子园矿床晚硫化物阶段闪锌矿、方铅矿及方解石的吻合较好(图4),表明2个矿床是从同一成矿流体中沉淀形成的产物。水头山矿床矿石矿物及矿石与围岩(碳酸盐岩)稀土元素特征略有不同,反映水头山矿床成矿物质主要来自深部岩浆的特征,这与芦子园矿床成矿物质来源相一致(邓明国等,2016)。

稀土元素Y与Ho因在价态、离子半径及配位数

表4 水头山矿床及芦子园矿床硫化物、矿石、围岩及岩体Y/Ho值对比表

Table 4 Contrast of Y/Ho ratios of sulfide, ore and wallrock of the Shuitoushan and Luziyuan deposit and rock body

名称	样品	样品数	最小值	最大值	平均值	数据来源
水头山Pb-Zn矿床	硫化物	8	8.5	53	28.287	
	矿石	2	30.833	33.182	32.008	本文
	围岩	2	16.818	19.636	18.227	
芦子园Pb-Zn矿床	硫化物	5	3.5	24.7	11.24	林冰霞, 2013;
	矿石	7	22.14	32.41	27.547	邓明国等, 2016
保山地块	区域花岗岩(柯街、志本山、漕涧)	8	24.528	29.63	26.214	陶琰等, 2010; 禹丽等, 2014
	现代海水		45	67		Bau et al., 1997;
弧后盆地			25	51		Bau and Dulski, 1999;
中大西洋洋脊			28	51		Douville et al., 1999
东太平洋洋脊			30	45		

等方面具有相似的地球化学行为,其Y/Ho值在大量地质作用过程中保持不变(Nozaki et al., 1997),所以Y/Ho值可以指示成矿流体的来源(Bau and Dulski, 1999; 章永梅等, 2014)。世界上大多数岩浆岩和碎屑沉积物(多为长英质和玄武质地壳)均保持着球粒陨石的Y/Ho值(24~34, 均值为28)(Nozaki et al., 1997; Bolhar et al., 2005)。水头山矿床矿石(30.833~33.182)及各类硫化物(主要集中在18.75~36.667)的Y/Ho值与芦子园矿床矿石Y/Ho

变化范围(22.14~32.41)十分相似(表4、图6),接近区域花岗岩(柯街、志本山及漕涧)变化范围(24.528~29.63)(陶琰等, 2010; 禹丽等, 2014),而与水头山矿床围岩变化范围(16.818~19.636)明显不同,这进一步证实2个矿床的成矿物质主要来自深部岩浆岩,这与前述稀土元素特征所得结论一致,亦与矿床地质特征吻合。

## 5.2 成矿流体来源与演化

C-O同位素组成可以示踪成矿热液中CO<sub>2</sub>的

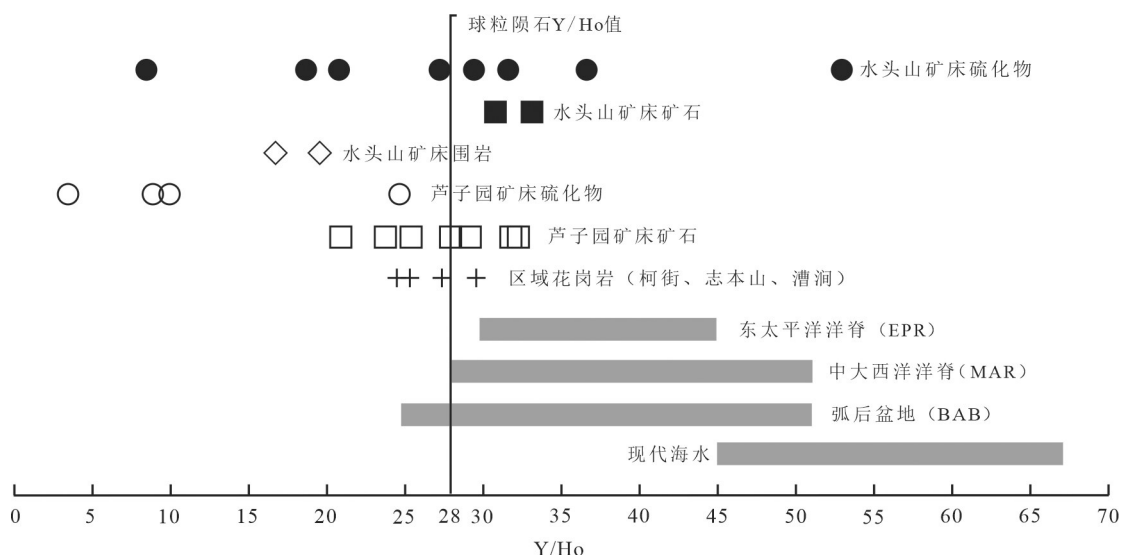


图6 水头山矿床、芦子园矿床及区域花岗岩Y/Ho值对比图

芦子园矿床矿石数据引自林冰霞, 2013; 芦子园矿床闪锌矿数据引自邓明国等, 2016; 柯街、志本山数据引自陶琰等, 2010; 漕涧数据引自禹丽等, 2014; EPR、MAR、BAB及现代海水数据引自 Bau et al., 1997; Bau and Dulski, 1999; Douville et al., 1999

Fig.6 Contrast of Y/Ho ratios of Shuitoushan, Luziyuan deposit and regional granite

The ore data of the Luziyuan deposit from Lin Bingxia, 2013; The zinc blende data of the Luziyuan deposit from Deng Mingguo et al., 2016; The data of Kejie and Zhibenshan from Tao Yan et al., 2010; The data of Caojian deposit from Yu Li et al., 2014; EPR, MAR, BAB and modern seawater data from Bau et al., 1997, Bau and Dulski, 1999, Douville et al., 1999

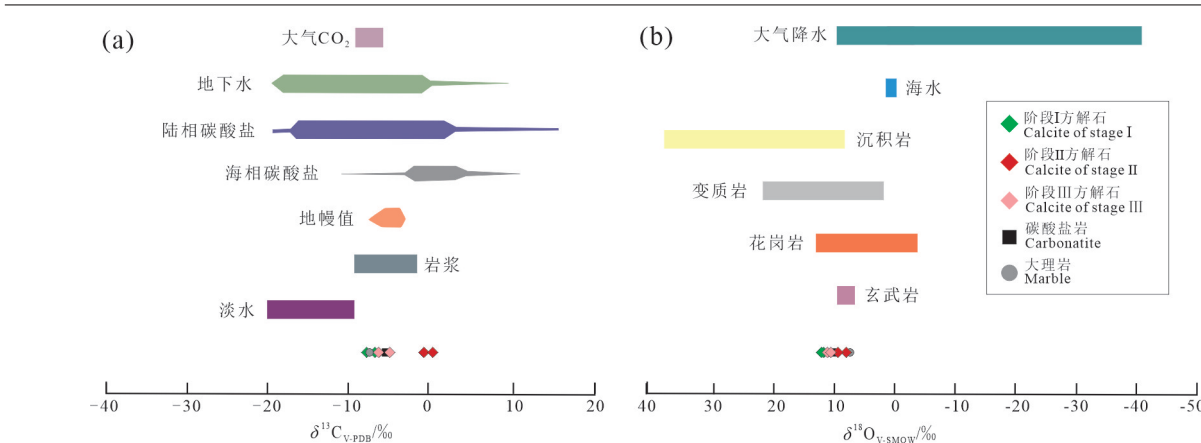


图7 重要地质储库C–O同位素特征(a底图据Clark and Fritz, 1997;b底图据Hoefs, 1997)

Fig.7  $\delta^{13}\text{C}_{\text{V-PDB}}$  and  $\delta^{18}\text{O}_{\text{V-SMOW}}$  values of important geological reservoirs (a after Clark and Fritz, 1997; b after Hoefs, 1997)

来源(Spangenberg et al., 1996; Zhou et al., 2013)。阶段Ⅰ方解石落入岩浆及陆相碳酸盐的分布范围内(图7a),同时与地幔值相近;阶段Ⅱ方解石的 $\delta^{13}\text{C}_{\text{V-PDB}}$ 值与海相碳酸盐、陆相碳酸盐的分布范围均有重叠之处(图7a),且靠近岩浆的 $\delta^{13}\text{C}_{\text{V-PDB}}$ 值;阶段Ⅲ方解石则落入陆相碳酸盐及岩浆的分布范围内(图7a),亦与地幔值相近,类似于碳酸盐岩地层。阶段Ⅱ方解石C–O同位素组成( $\delta^{13}\text{C}_{\text{V-PDB}}$ 值为-0.6‰~0.5‰, $\delta^{18}\text{O}_{\text{V-SMOW}}$ 值为11.4‰~12‰)与镇康矿集区内芦子园矿床晚硫化物阶段的C–O同位素组成( $\delta^{13}\text{C}_{\text{V-PDB}}$ 值为-1.0‰~0.9‰, $\delta^{18}\text{O}_{\text{V-SMOW}}$ 值为10.3‰~12.7‰)吻合较好(Xu et al., 2019),表明两个矿床的成矿流体具有同源性,为同一成矿流体形成的产物。水头山矿床各样品的 $\delta^{18}\text{O}_{\text{V-SMOW}}$ 值(7.59‰~12.2‰)较为一致,投点均落于花岗岩、变质岩及沉积岩的分布范围内,且靠近大气降水(图7b)。此外,水头山矿床阶段Ⅱ闪锌矿、方铅矿及方解石样品的轻稀土相对富集,其稀土元素配分模式十分相近,亦分别与芦子园矿床晚硫化物阶段闪锌矿、方铅矿及方解石的吻合较好(图4),亦表明两个矿床可能具有相似的成矿流体REE来源,且成矿过程中其REE组成无显著变化。综上所述,水头山矿床的碳质可能与深部岩浆活动有关,这与芦子园矿床成矿流体来源相吻合(邓明国等,2017)。

在热液矿床中,碳酸盐矿物方解石的低 $\delta^{13}\text{C}_{\text{V-PDB}}$ 值通常指示碳来自深源(Chen et al., 2004; Goldfarb et al., 2004)。综合图7与图8,并考虑到保山地块不具备原生碳酸盐的形成条件,且H、O同位素表明该

矿床发生的成矿作用与深部岩浆活动密切相关,这与S、Pb同位素所得到的结论基本一致(邓明国等,2017),从而进一步证实该矿床碳质主要来自深部岩浆岩,前期成矿热液运移中有沉积岩混染,随着成矿作用的进行, $\delta^{13}\text{C}_{\text{V-PDB}}$ 和 $\delta^{18}\text{O}_{\text{V-SMOW}}$ 值逐渐降低,后期受低温蚀变作用与大气降水的影响相当明显,因此阶段Ⅱ方解石的 $\delta^{13}\text{C}_{\text{V-PDB}}$ 、 $\delta^{18}\text{O}_{\text{V-SMOW}}$ 值均比阶段Ⅰ、Ⅲ阶段方解石高的原因(表3)。与典型海相碳酸盐( $\delta^{13}\text{C}_{\text{V-PDB}} = -4\text{\textperthousand} \sim 4\text{\textperthousand}$ ,  $\delta^{18}\text{O}_{\text{V-SMOW}} = 20\text{\textperthousand} \sim 24\text{\textperthousand}$ )(Hoefs, 1997)相比,水头山矿床一个明显的特征就是所有样品的 $\delta^{18}\text{O}_{\text{V-SMOW}}$ 值明显偏低;阶段Ⅱ方解石 $\delta^{13}\text{C}_{\text{V-PDB}}$ 值正常,而阶段Ⅰ、Ⅲ阶段方解石 $\delta^{13}\text{C}_{\text{V-PDB}}$ 值与碳酸盐岩地层相近,但略有亏损。

综上所述,水头山矿床成矿流体主要来源于深部岩浆岩,该矿床的形成可能是随着中特提斯怒江洋的闭合,保山地块与腾冲地块发生碰撞挤压加厚作用使地壳重熔,在保山地块镇康矿集区深部形成隐伏中酸性岩浆;在碰撞期内发生幕式剪切拉张作用,使深部中酸性岩浆沿断裂上涌,上涌过程中萃取的矿质融入早期的成矿流体中,成矿流体在运移过程中,与沉积岩发生混染作用;成矿流体沿幕式伸展形成的张性裂隙运移,与大气降水混合形成含矿热液流体,在远离隐伏中酸性岩体的构造裂隙中金属硫化物沉淀富集,形成似层状和透镜体的矿体。

### 5.3 矿床成因

水头山矿床所处的保山地块其结晶基底为震旦系—中寒武统公养河群的变质砂板岩,向顶部过渡为云母质砂岩和页岩组成的复理石韵律沉积旋

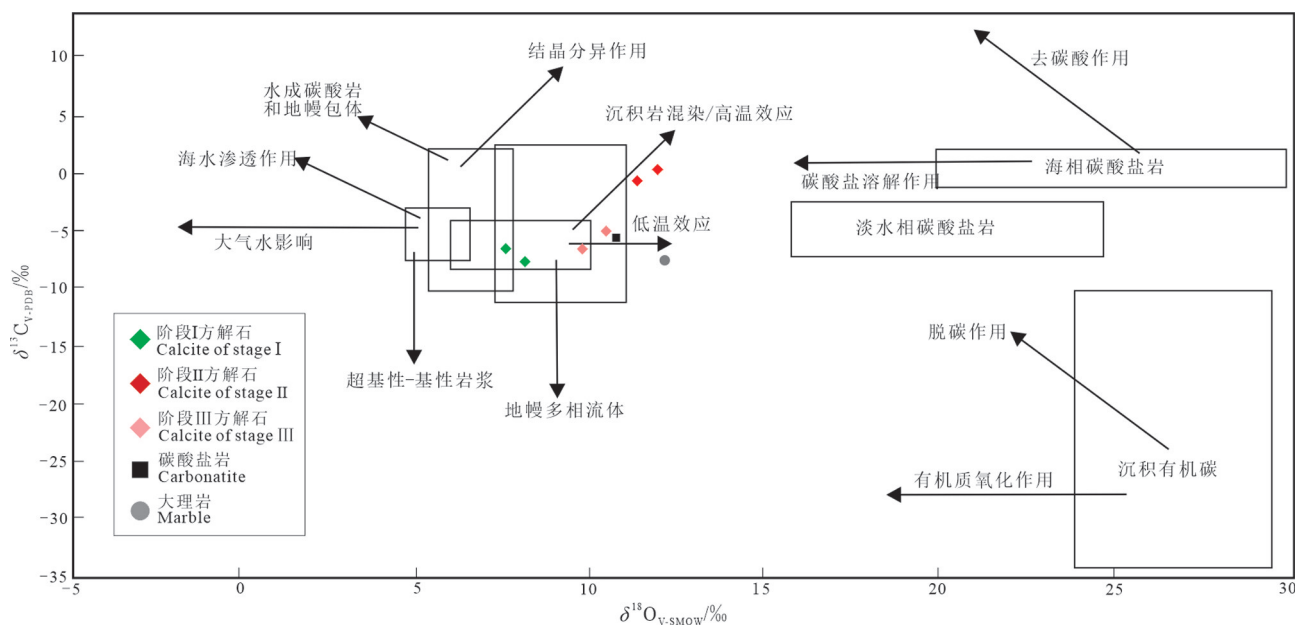
图8 水头山矿床  $\delta^{13}\text{C}_{\text{V}-\text{PDB}}-\delta^{18}\text{O}_{\text{V}-\text{SMOW}}$  图解(底图据王长明等, 2007; 周家喜等, 2012; 袁波等, 2014)

Fig. 8  $\delta^{13}\text{C}_{\text{V}-\text{PDB}}-\delta^{18}\text{O}_{\text{V}-\text{SMOW}}$  diagram of the Shuitoushan Pb-Zn deposit (after Wang Changming et al., 2007; Zhou Jiaxi et al., 2012; Yuan Bo et al., 2014)

回,而盖层为晚寒武世以来沉积的半深海—滨海相泥砂岩质和碳酸盐岩建造(黄勇等, 2012; Burchfiel and Chen, 2012)。震旦纪—中寒武世形成基底以后,转为晚寒武世—晚石炭世冈瓦纳大陆沉积阶段,经历了早二叠世萨克马尔期末陆内裂解作用过程,随后由于晚三叠世至早白垩世中特提斯主洋闭合作用的影响,保山地块南部地区及其周缘进入了碰撞造山阶段,其内部则遭受了强烈的陆内变形作用(莫宣学和潘桂棠, 2006; Metcalfe, 2011; Deng et al., 2014b),并在燕山晚期逐渐增强,最终定形于喜山期。区块内志本山、柯街及漕涧S型花岗岩的产出,该类型花岗岩具有高钾过铝质性质,是由于地壳碰撞加厚及阶段性剪切拉张引起地壳重熔形成(陶琰等, 2010),反映了保山地块内部可能存在地壳和岩石圈的幕式剪切拉张(毛景文等, 2005; 邓明国等, 2016);怒江大断裂与柯街—南汀河大断裂强烈的活动使该区地质构造错综复杂,多处形成了“X”状裂隙。本矿床位于镇康复背斜南倾伏端及与之配套的NEE向次级乌木兰背斜的复合部位,因经历多期次构造运动,最终形成由NEE向和NW向两组断裂构成的“X”型共轭断裂格架,且矿石角砾状构造、梳状构造、晶洞构造较发育,表明该矿床可能形成于体系相对开放的构造环境中。

水头山矿床矿体呈似层状、透镜状赋存于大理岩化灰岩和构造角砾岩中,矿石矿物组成较简单,主要以闪锌矿和方铅矿为主,偶见少许黄铜矿、黄铁矿等,脉石矿物以方解石为主的一套低温热液成因的矿物组合;围岩蚀变有方解石化、白云石化、绿泥石化、硅化和绢云母化等中低温热液蚀变特点。上述矿石组构和蚀变特征记录了该矿床成矿流体的迁移和演化等方面的重要信息,暗示其具有典型的中低温热液成因特征(林方成, 2005a, 2005b; 杨向荣等, 2009)。

综上讨论,水头山的成矿物质来源和成矿流体演化及来源可概括为:①稀土元素含量及比值反映成矿物质主要来源于深部岩浆岩;②C-O同位素组成表明成矿流体主要来源于深部的岩浆热液,前期成矿流体在运移过程中可能有沉积岩的混染,后期可能受到低温蚀变和大气降水的影响。同时前人利用地物化遥等资料综合推测矿区深部存在隐伏中酸性岩体(李开闭等, 2012; 吾守艾力·肉孜等, 2015; Liang et al., 2015)。因此,笔者认为水头山矿床产出位置受成岩后断裂控制,矿体形态以似层状或透镜状为主,Pb-Zn矿是在阶段Ⅱ形成,矿石的沉淀明显晚于碳酸盐岩,与隐伏中酸性岩体有关的热液成矿作用可能是导致该矿床阶段Ⅱ方解石和

Pb-Zn矿沉淀的主导因素。结合区域地质及地球化学特征认为,该矿床是在陆陆碰撞、陆内挤压和剪切拉张的构造背景下,地壳缩短、加厚重熔产生的岩浆热液远距离效应的产物。将水头山矿床与相距仅6 km的芦子园超大型Pb-Zn-Fe-Cu多金属矿床进行对比,从芦子园矿床到水头山矿床的地质特征呈现出由矽卡岩型Pb-Zn-Fe矿化逐渐过渡到低温热液型Pb-Zn矿化的特征。两矿床矿化带的海拔高度分别为2050 m和1750 m,主要控矿构造均为同期形成的NE、NEE向两组断裂,表明两矿床可能为同一构造热液体系的产物。尽管两个矿床矿化类型和同位素体系不尽相同,但水头山矿床阶段Ⅱ与芦子园矿床晚硫化物阶段在地质特征和地球化学特征方面具有很好的吻合性,为同一成矿流体形成的产物。此外水头山矿床的地质特征和地球化学特征与甲乌拉、查干布拉根等典型低温热液型矿床(Hedenquist and Lowenstern, 1994; Li et al., 2015, 2016)非常相似。因此,认为水头山矿床为芦子园超大型矽卡岩矿床伴生的、矿化相对较浅的,与深部中酸性岩浆热液成矿作用有关的低温热液型矿床。

## 6 结 论

(1) 水头山矿床矿石的稀土元素特征与单矿物稀土元素配分模式相似,亦与保山地块内燕山期花岗岩(柯街和志本山)吻合较好,而与围岩微量稀土元素特征略有不同,表明该矿床成矿流体中REE主要来源于深部岩浆热液。同时该矿床矿石、硫化物的Y/Ho值与柯街、志本山、漕涧花岗岩较为一致,与水头山矿床围岩明显不同,进一步表明该矿床的成矿物质主要来源于深部岩浆热液。

(2) C-O同位素分析结果表明水头山矿床的成矿流体主要来源于深部的岩浆热液,前期成矿流体在运移过程中可能有沉积岩的混染,后期可能受到低温蚀变和大气降水的影响。综合区域地质、矿床地质特征和矿床地球化学认为,该矿床的形成是与区内深部隐伏花岗岩成矿作用有关的低温热液矿床。

**致谢:**野外工作得到云南兴达矿业有限公司的大力支持和帮助;北京核工业地质研究院稳定同位素实验室刘牧老师和中国科学技术大学地球与空间科学学院固体同位素地球化学实验室陈福坤老师对实验进行了认真指导,审稿专家对论文提出了

宝贵的修改意见,在此一并表示感谢!

## 注释

- ① 云南省地质调查院. 2016. 云南省镇康县水头山铅锌矿勘探报告[R]. 1-211.

## References

- Bau M, Mller P, Dulski P. 1997. Yttrium and lanthanides in eastern Mediterranean seawater and their fractionation during redox-cycling[J]. Marine Chemistry, 56: 123-131.
- Bau M, Dulski P. 1999. Comparing yttrium and rare earths in hydrothermal fluids from the Mid-Atlantic Ridge: Implications for Y and REE behavior during near-vent mixing and for the Y/Ho ratio of Proterozoic seawater [J]. Chemical Geology, 155: 77-90.
- Bolhar R, Van Kranendonk M J, Kamber B S. 2005. A trace element study of siderite-jasper banded iron formation in the 3.45 Ga Warrawoona Group, Pilbara Craton-formation from hydrothermal fluids and shallow seawater [J]. Precambrian Research, 137(1/2): 93-114.
- Burchfiel B C, Chen Z L. 2012. Tectonics of the southeastern Tibetan Plateau and its adjacent foreland[J]. Geological Society of America Memoir, 210: 1-164.
- Chen Fuchuan. 2018. The Study of Early Cretaceous Skarn Mineralization in Longyang Ore Concentration Area, Baoshan Block, Sanjiang Region, SW China[D]. Beijing: China University of Geosciences, 1-142 (in Chinese with English abstract).
- Chen F K, Li X H, Wang X L, Li Q L, Siebel W. 2007. Zircon age and Nd-Hf isotopic composition of the Yunnan Tethyan belt, southwestern China[J]. International Journal of Earth Sciences, 96 (6): 1179-1194.
- Chen Mingyong. 2014. Geological features and prospecting criteria of the Shuitoushan lead zinc deposit in Zhenkang County, Yunnan Province[J]. Low Carbon World, 4: 117-118 (in Chinese).
- Chen Y J, Zhao Y C. 1997. Geochemical characteristics and evolution of REE in the Early Precambrian sediments: Evidences from the southern margin of the North China craton[J]. Episodes, 20: 109-116.
- Chen Y J, Pirajno F, Sui Y H. 2004. Isotope geochemistry of the Tieluping silver deposit, Henan, China: A case study of orogenic silver deposits and related tectonic setting[J]. Mineralium Deposita, 39: 560-575.
- Clark I D, Fritz P. 1997. Environmental Isotopes in Hydrogeology[M]. New York: Lewis Publishers, 1-342.
- Deng J, Wang Q F, Li G J, Santosh M. 2014a. Cenozoic tectono-magmatic and metallogenic processes in the Sanjiang region, southwestern China[J]. Earth-Science Reviews, 138: 268-299.
- Deng J, Wang Q F, Li G J, Li C S, Wang C M, 2014b. Tethys tectonic evolution and its bearing on the distribution of important mineral deposits in the Sanjiang region, SW China[J]. Gondwana Research,

- 26(2): 419–437.
- Deng Mingguo, Xu Rong, Wang Peng, Sun Baidong, Zeng Lei, Yu Haijun, Wang Tao, Sha Jianze. 2016. Geochemistry of the rhodonite in the Luziyuan Pb–Zn–Fe polymetallic deposit in West Yunnan and their genesis significance[J]. *Acta Petrologica Sinica*, 32(8): 2248–2264 (in Chinese with English abstract).
- Deng Mingguo, Zhao Jianxing, Liu Fengxiang, Yu Haijun, Sun Baidong, Liu Fei, Li shibin. 2017. Discussion on sources of metallogenetic fluids and materials of Shuitoushan Pb–Zn deposits in Zhenkang, western Yunnan: Evidence from H, O, S and Pb isotopes[J]. *Acta Petrologica Sinica*, 33(7): 2001–2017 (in Chinese with English abstract).
- Ding Weipin, Xie Caifu, Huang Cheng, Zhang Bin, Xin Zhuo, Zhan Huasi, Zheng Lilong, Kong Fanquan, Wang Hongbing, Huang Fulin. 2022. Sources of Permian lead–zinc ore-forming materials in Sichuan–Yunnan–Guizhou area: C–H–O–S–Pb isotope constraints—An example from Taipingzi lead–zinc deposit in Yunnan Provinces[J]. *Geology in China*, 49(6): 1845–1861 (in Chinese with English abstract).
- Dong M L, Dong G C, Mo X X, Santosh M, Zhu D C, Yu J C, Nie F, Hu Z C. 2013. Geochemistry, Zircon U–Pb geochronology and Hf isotopes of granites in the Baoshan Block, western Yunnan: Implications for Early Paleozoic evolution along the Gondwana margin[J]. *Lithos*, 179: 36–47.
- Douville E, Bienvenu P, Charlou J. 1999. Yttrium and rare earth elements in fluids from various deep-sea hydrothermal systems[J]. *Geochimica et Cosmochimica Acta*, 63: 627–643.
- Friedman I, O’Neil J R. 1977. Complication of Stable Isotope Fractionation Factors of Geochemical interest in Data of Geochemical Interest in Data of Geochemistry. In: Fleischer M (ed.). *Geological Professional Paper*[M]. Virginia: U.S. Geological Survey, 6: 1–440.
- Goldfarb R J, Ayuso R, Miller M L, Ebert S W, Marsh E E, Petsel S A, Miller L D, Bradley D, Johnson C, McClelland W. 2004. The Late Cretaceous Donlin Creek gold deposit, Southwestern Alaska: Controls on epizonal ore forming [J]. *Economic Geology*, 99: 643–671.
- Henderson P. 1984. *Rare Earth Element Geochemistry*[M]. Amsterdam: Elsevier Science Publishers.
- Hedenquist J W, Lowenstern J B. 1994. The role of magmas in the formation of hydrothermal ore deposit[J]. *Nature*, 37(18): 519–527.
- Hoefs J. 1997. *Stable Isotope Geochemistry* (4th Edition)[M]. Berlin: Springer Verlag, 1–201.
- Huang Hua, Zhang Changqing, Zhou Yunman, Xie Huafeng, Liu Bo, Xie Yongfu, Dong Yuntao, Yang Chunhai, Dong Wenwei. 2014. Rb–Sr isochron age of Jinchanghe Fe–Cu–Pb–Zn polymetallic deposit in Yunnan Province and its geological significance[J]. *Mineral Deposits*, 33(1): 123–136 (in Chinese with English abstract).
- Huang Yong, Hao Jiaxu, Bai Long, Deng Guibiao, Zhang Guoxiang, Huang Wenjun. 2012. Stratigraphic and petrologic response to Late Pan–African movement in Shidian area, western Yunnan Province[J]. *Geological Bulletin of China*, 31(2/3): 306–313 (in Chinese with English abstract).
- Huang Z L, Li X B, Zhou M F, Li W B, Jin Z G. 2010. REE and C–O isotopic geochemistry of calcites from the world-class Huize Pb–Zn deposits, Yunnan, China: Implications for the ore genesis [J]. *Acta Geologica Sinica*, 84(3): 597–613.
- Kerrick R, Goldfarb R J, Groves D, Garwin S, Jia Y F. 2000. The characteristics, origins, and geodynamic settings of supergiant gold metallogenetic provinces[J]. *Science in China (Series D)*, 43: 1–68.
- Li Kaibi, Yang Shusheng, Cai Xu. 2012. The effect and result of high-precision magnetic survey on prospecting in Luziyuan mine in Zhenkang Country[J]. *Journal of Yunnan University (Natural Sciences)*, 34(S2): 157–162 (in Chinese with English abstract).
- Li W B, Huang Z L, Qi L. 2007. REE geochemistry of sulfides from the Huize Zn–Pb ore field, Yunnan Province: Implication for the sources of ore-forming metals[J]. *Acta Geologica Sinica*, 81(3): 442–449.
- Li Zhiqun, Chen Yaoguang, Zhang Taishen, Ren Zhiji, Zhao Chongshun, Li Weizhong. 2005. Geological characters and sustainable mineral resources of Mengnuo Pb–Zn ore deposit in Yunnan[J]. *Contributions To Geology and Mineral Resources Research*, 20: 123–131 (in Chinese with English abstract).
- Li T G, Wu G, Liu J, Hu Y Q, Zhang Y F, Luo D F, Mao Z H. 2015. Fluid inclusions and isotopic characteristics of the Jiawula Pb–Zn–Ag deposit, Inner Mongolia, China[J]. *Journal of Asian Earth Sciences*, 103: 305–320.
- Li T G, Wu G, Liu J, Wang G R, Hu Y Q, Zhang Y F, Luo D F, Mao Z H, Xu B. 2016. Geochronology, fluid inclusions and isotopic characteristics of the Chaganbulagen Pb–Zn–Ag deposit, Inner Mongolia, China[J]. *Lithos*, 261: 340–355.
- Liang S X, Jiao Y J, Guo J. 2015. Prediction of hidden granites in the Luziyuan area of Yunnan Province and the prospecting direction[J]. *Acta Geological Sinica (English Edition)*, 89(5): 1781–1782.
- Liao Shiyong, Wang Dongbing, Tang Yuan, Yin Fuguang, Sun Zhiming, Sun Jie. 2013. LA–ICP–MS U–Pb age of two-mica granite in the Yunlong tin–tungsten metallogenetic belt in Three river region and its geological implications [J]. *Acta Petrologica et Mineralogica*, 32(4): 450–462 (in Chinese with English abstract).
- Lin Bingxia. 2013. Research on Geological and Geochemical Features of Pb–Zn Deposit in Luziyuan, Zhenkang, Yunnan Province[D]. Kunming: Kunming University of Science and Technology (in Chinese with English summary).
- Lin Fangcheng. 2005a. Typical ore fabrics of Heiqu–Xuequ stratiform lead–zinc deposit in Hanyuan, Sichuan, and their genetic implications[J]. *Mineral Deposits*, 24(2): 122–133 (in Chinese with English abstract).
- Lin Fangcheng. 2005b. Geological and geochemical characteristics and genesis of supper-large-scale sedex-type stratiform lead–

- zinc deposits in the Dadu river valley on the western margin of the Yangtze craton[J]. *Acta Geologica Sinica*, 79(4): 540– 556 (in Chinese with English abstract).
- Liu S, Hu R Z, Gao S, Feng C X, Huang Z L, Lai S C, Yuan H L, Liu X M, Coulson I M, Feng G Y, Wang T, Qi Y Q. 2009. U–Pb zircon, geochemical and Sr–Nd–Hf isotopic constraints on the age and origin of Early Palaeozoic I–type granite from the Tengchong–Baoshan block, western Yunnan Province, SW China[J]. *Journal of Asian Earth Sciences*, 36(2/3): 168–182.
- Liu Jinkang, Deng Mingguo, Li Yuhua, Liu Yang. 2020. The ICP–MS trace element characteristics of sphalerites from the Mengxing Pb–Zn deposit, western Yunnan and their geological significances[J]. *Bulletin of Mineralogy, Petrology and Geochemistry*, 39(1): 133–143 (in Chinese with English abstract).
- Liu Xuelong, Li Wenchang, Zhou Yunman, Zhao Chengfeng, Wang Jiyan, Li Qingrui, Li Shoukui, Wang Hai, Lu Bode, Zhou Jiehu, Li Fanglan, Liu Xue. 2022. Metallogenesis system of polymetallic Fe–Cu–Au–Pb–Zn deposits in Jinchanghe ore concentration district, Baoshan block, Southwest China[J]. *Sedimentary Geology and Tethyan Geology*, 42(1): 133–150 (in Chinese with English abstract).
- Long Hansheng, Luo Taiyi, Huang Zhilong, Zhou Mingzhong, Yang Yong, Qian Zhikuan. 2011. Rare earth element and trace element geochemistry of Pyrite ores in the Laochang large size silver polymetallic deposit of Lancang, Yunnan Province, China[J]. *Acta Mineralogical Sinica*, 31(3): 462–473 (in Chinese with English abstract).
- Lottermoser B G. 1989. Rare earth element study of exhalites within the Willyama supergroup, Broken Hill Block, Australia[J]. *Mineralium Deposita*, 24(2): 92–99.
- Mao Jingwen, Wang Zhiliang, Li Houmin, Wang Chengyu, Chen Yuchuan. 2003. Carbon and oxygen isotope components in the Permian basalt–hosted copper deposits in Ludian area, Yunnan: Implication for the mineralization process[J]. *Geological Review*, 49(6): 610–615 (in Chinese with English abstract).
- Mao Jingwen, Xie Guiqing, Li Xiaofeng, Zhang Zuoheng, Wang Yitian, Wang Zhiliang, Zhao Shengcai, Yang Fuquan, Li Houmin. 2005. Geodynamic process and metallogeny: History and present research trend, with a special discussion on continental accretion and related metallogeny throughout geological history in South China[J]. *Mineral Deposits*, 24(3): 193–205 (in Chinese with English abstract).
- Metcalfe I. 2011. Tectonic framework and Phanerozoic evolution of Sundaland[J]. *Gondwana Research*, 19(1): 3–21.
- Metcalfe I. 2013. Gondwana dispersion and Asian accretion: Tectonic and palaeogeographic evolution of eastern Tethys[J]. *Journal of Asian Earth Science*, 66: 1–33.
- Michard A. 1989. Rare earth element systematics in hydrothermal fluids[J]. *Geochimica et Cosmochimica Acta*, 53(3): 745–750.
- Mo Xuanxue, Pan Guitang. 2006. From the Tethys to the formation of the Qinghai–Tibet Plateau: Constrained by tectono–magmatic events[J]. *Earth Science Frontiers*, 13(6): 43–51 (in Chinese with English abstract).
- Nie Fei, Dong Guochen, Mo Xuanxue, Zhao Zhidan, Wang Peng, Cui Ziliang, Fan Wenyu, Liu Shusheng. 2015. The characteristics of sulfur and lead isotopic compositions of the Xiyi Pb–Zn deposit in Baoshan Block, western Yunnan[J]. *Acta Petrologica Sinica*, 31(5): 1327–1334 (in Chinese with English abstract).
- Nozaki Y, Zhang J, Amakawa H. 1997. The fractionation between Y and Ho in the marine environment[J]. *Earth and Planetary Science Letters*, 148: 328–341.
- Pang Xucheng, Zhu Haofeng, HU Ruizhong, Zong Jing. 2010. REE geochemical character of the Baoertu copper deposit in Xinjiang and its geological significance[J]. *Geology in China*, 37(6): 1699–1709 (in Chinese with English abstract).
- Spangenberg J E, Fontboté L, Sharp Z D, Hunziker J. 1996. Carbon and oxygen isotope study of hydrothermal carbonates in the zinc–lead deposits of the San Vicente district, central Peru: A quantitative modeling on mixing processes and CO<sub>2</sub> degassing[J]. *Chemical Geology*, 133(1/4): 289–315.
- Tao Yan, Hu Ruizhong, Zhu Feilin, Ma Yangsheng, Ye Lin, Cheng Zengtao. 2010. Ore-forming age and the geodynamic background of the Hetaoping Lead–Zinc deposit in Baoshan, Yunnan[J]. *Acta Petrologica Sinica*, 26(6): 1760–1772 (in Chinese with English abstract).
- Taylor S R, McLennan S M. 1985. *The Continental Crust: Its Composition and Evolution*[M]. Oxford: Blackwel.
- Wang Changming, Zhang Shouting, Deng Jun, Liu Jianming. 2007. The exhalative genesis of the stratabound skarn in the Huanggangliang Sn–Fe polymetallic deposit of Inner Mongolia[J]. *Acta Petrologica et Mineralogica*, 26(5): 409–417 (in Chinese with English abstract).
- Wang Liqiang, Cheng Wenbin, Luo Maocheng, Xiang Haoyu. 2012. A study of metallic sulfides, quartz REE composition characteristics and genesis of the Mengya's lead–zinc deposit [J]. *Geology in China*, 39(3): 740–749 (in Chinese with English abstract).
- Wang Zhonggang, Yu Xueyuan, Zhao Zhenhua. 1989. *Rare Earth Element Geochemistry*[M]. Beijing: Science Press, 1–11 (in Chinese with English abstract).
- Wu Shouaili · rouzi, Liang Shengxian, Zou Guangfu, Luo Maojin. 2015. The application of AMT and 3D gravity methods to the prospecting for concealed rock body in the Luziyuan area[J]. *Geophysical and Geochemical Exploration*, 39(3): 525–529 (in Chinese with English abstract).
- Xia Qinglin, Chen Yongqing, Lu Yingxiang, Jiang Chengxing, Liu Honghuang, Lü Zhicheng. 2005. Geochemistry, fluid inclusion, and stable isotope studies of Luziyuan Pb–Zn deposit in Yunnan Province, southwestern China[J]. *Earth Science*, 30(2): 177–186.

- (in Chinese with English abstract).
- Xiang Shihong, Xue Chunji, Cao Jihu, Zhang Xu, Li Yongfeng, Li Bingqi. 2013. Characteristics and geological significance of C, O isotopes of calcite in the Yindonggou Pb-Zn-Ag deposit, north Neixiang, Henan Province[J]. Bulletin of Mineralogy, Petrology and Geochemistry, 32(3): 364–369 (in Chinese with English abstract).
- Xiao Changhao. 2013. Study on Minerogenic Series of Epithermal Deposits in Mid-Southern Segment of the Sanjiang Orogenic Belt, Southwest China[D]. Beijing: China University of Geosciences, 1–153 (in Chinese with English abstract).
- Xu R, Li W C, Deng M G, Zhou J X, Ren T, Yu H J. 2019. Genesis of the superlarge Luziyuan Zn-Pb-Fe(-Cu) distal skarn deposit in western Yunnan (SW China): Insights from ore geology and C-H-O-S isotopes[J]. Ore Geology Reviews, 107: 944–959.
- Yang Fei. 2015. Metallogenic Geological Background and Geological Characteristics of the Wengkong Lead Zinc Mine in Zhenkang County, Yunnan Province[D]. Beijing: China University of Geosciences, 1–59 (in Chinese with English abstract).
- Yang L, Wang Q F, Liu H, Carranza E, Li G J, Zhou D Q. 2016. Identification and mapping of geochemical patterns and their significance for regional metallogeny in the southern Sanjiang, China [J]. Ore Geology Reviews, 90: 1042–1053.
- Yang Xiangrong, Peng Jiantang, Hu Ruizhong, Qi Huawei, Liu Shen. 2009. Characteristics and genesis of ore tube stureture of Tamu zinc-lead deposit, southwest margin of Tarim Basin, Xinjiang[J]. Acta Petrologica Sinica, 25(4): 977–983 (in Chinese with English abstract).
- Yang Y L, Ye L, Cheng Z T, Bao T. 2013. Origin of fluids in the Hetaoping Pb-Zn deposit, Baoshan-Narong-Dongzhi block metallogenic belt, Yunnan Province, SW China[J]. Journal of Asian Earth Sciences, 73: 362–371.
- Yu Li, Li Gongjian, Wang Qingfei, Liu Xuefei. 2014. Petrogenesis and tectonic significance of the Late Cretaceous magmatism in the northern part of the Baoshan block: Constraints from bulk geochemistry, zircon U-Pb geochronology and Hf isotopic compositions[J]. Acta Petrologica Sinica, 30(9): 2709–2724 (in Chinese with English abstract).
- Yuan Bo, Mao Jingwen, Yan Xinghu, Wu Yue, Zhang Feng, Zhao Liangliang. 2014. Sources of metallogenic materials and metallogenic mechanism of Daliangzi Ore Field in Sichuan Province: Constraints from geochemistry of S, C, H, O, Sr isotope and trace element in sphalerite[J]. Acta Petrologica Sinica, 30(1): 209–220 (in Chinese with English abstract).
- Zhang Chuanyu, Li Wenchang, Yu Haijun, Li Wanting, Luo Jianhong, Sha Jianze, Wu Qinghua, Pan Zewei. 2022. Sphalerites Rb-Sr Dating and geological significance of the Shuitoushan Pb-Zn deposit in Yunnan Province, SW China[J]. Sedimentary Geology and Tethyan Geology, 42(1): 122–132 (in Chinese with English abstract).
- Zhang Yongmei, Gu Xuexiang, Peng Yiwei, Zheng Luo, Zhang Yan, Gao Haijun, Dong Shuyi. 2014. Geology, geochemistry and genesis of the Bonga carbonatite-type niobium deposit, Angola[J]. Earth Science Frontiers, 21(5): 50–68 (in Chinese with English abstract).
- Zhou Jiaxi, Huang Zhilong, Zhou Guofu, Jin Zhongguo, Li Xiaobiao, Ding Wei, Gu Jing. 2010. Sources of ore metals of the Tianqiao Pb-Zn deposit in northwestern Guizhou Province: Constraints from S, Pb isotope and REE geochemistry[J]. Geological Review, 56(4): 513–524 (in Chinese with English abstract).
- Zhou Jiaxi, Huang Zhilong, Zhou Guofu, Zeng Qiaosong. 2012. C, O isotope and REE geochemistry of the hydrothermal calcite from the Tianqiao Pb-Zn ore deposit in NW Guizhou Province, China[J]. Geotectonica et Metallogenesis, 36(1): 93–101 (in Chinese with English abstract).
- Zhou J X, Huang Z L, Zhou M F, Li X B, Jin Z G. 2013. Constraints of C-O-S-Pb isotope compositions and Rb-Sr isotopic age on the origin of the Tianqiao carbonate-hosted Pb-Zn deposit, SW China[J]. Ore Geology Reviews, 53: 77–92.

## 附中文参考文献

- 陈福川. 2018. 西南三江保山地块珑阳矿集区早白垩世矽卡岩矿床成矿作用研究[D]. 北京: 中国地质大学, 1–142.
- 陈明勇. 2014. 云南省镇康县水头山铅锌矿地质特征及找矿标志探讨[J]. 低碳世界, 4: 117–118.
- 邓明国, 徐荣, 王朋, 孙柏东, 曾磊, 余海军, 王涛, 沙建泽. 2016. 滇西芦子园 Pb-Zn-Fe 多金属矿床蔷薇辉石地球化学特征及其成因意义[J]. 岩石学报, 32(8): 2248–2264.
- 邓明国, 赵剑星, 刘凤祥, 余海军, 孙柏东, 刘飞, 李仕斌. 2017. 滇西镇康水头山 Pb-Zn 矿床成矿流体及矿质来源探讨——H、O、S、Pb 同位素地球化学证据[J]. 岩石学报, 33(7): 2001–2017.
- 丁伟品, 谢财富, 黄诚, 张斌, 辛卓, 詹华思, 郑立龙, 孔凡全, 王红兵, 黄福林. 2022. 川滇黔二叠系铅锌成矿物质来源:C-H-O-S-Pb 同位素制约——以云南太平子铅锌矿为例[J]. 中国地质, 49(6): 1845–1861.
- 黄华, 张长青, 周云满, 谢华锋, 刘博, 谢永富, 董云涛, 杨春海, 董文伟. 2014. 云南保山金厂河铁铜铅锌多金属矿床 Rb-Sr 等时线测年及其地质意义[J]. 矿床地质, 33(1): 123–136.
- 黄勇, 郝家栩, 白龙, 邓贵标, 张国祥, 黄文俊. 2012. 滇西施甸地区晚泛非运动的地层学和岩石学响应[J]. 地质通报, 31(2/3): 306–313.
- 李开毕, 杨淑胜, 蔡旭. 2012. 高精度磁测在镇康芦子园矿区勘查中的作用及效果[J]. 云南大学学报(自然科学版), 34(S2): 157–162.
- 李志群, 陈耀光, 张泰身, 任治机, 赵重顺, 李伟中. 2005. 云南勐糯铅锌矿的成矿地质特征和资源接替[J]. 地质找矿论丛, 20: 123–131.
- 廖世勇, 王冬兵, 唐渊, 尹福光, 孙志明, 孙洁. 2013. “三江”云龙锡(钨)成矿带晚白垩世二云母花岗岩 LA-ICP-MS 锆石 U-Pb 定年及其地质意义[J]. 岩石矿物学杂志, 32(4): 450–462.
- 林冰霞. 2013. 云南省镇康县芦子园铅锌矿床地质地球化学特征研究[D]. 昆明: 昆明理工大学.

- 林方成. 2005a. 四川汉源黑区-雪区层状铅锌矿床典型矿石组构与成因[J]. 矿床地质, 24(2): 122-133.
- 林方成. 2005b. 扬子地台西缘大渡河谷超大型层状铅锌矿床地质地球化学特征及成因[J]. 地质学报, 79(4): 540-556.
- 刘锦康, 邓明国, 李余华, 刘阳. 2020. 滇西勐兴铅锌矿床闪锌矿ICP-MS微量元素特征及其地质意义[J]. 矿物岩石地球化学通报, 39(1): 133-143.
- 刘学龙, 李文昌, 周云满, 赵成峰, 王基元, 李庆锐, 李守奎, 王海, 陆波德, 周杰虎, 李方兰, 刘雪. 2022. 滇西保山地块金厂河矿集区铁铜金铅锌多金属矿床成矿系统[J]. 沉积与特提斯地质, 42(1): 133-150.
- 龙汉生, 罗泰义, 黄智龙, 周明忠, 杨勇, 钱志宽. 2011. 云南澜沧老厂大型银多金属矿床黄铁矿稀土和微量元素地球化学[J]. 矿物学报, 31(3): 462-473.
- 毛景文, 王志良, 李厚民, 王成玉, 陈毓川. 2003. 云南鲁甸地区二叠纪玄武岩中铜矿床的碳氧同位素对成矿过程的指示[J]. 地质论评, 49(6): 610-615.
- 毛景文, 谢桂青, 李晓峰, 张作衡, 王义天, 王志良, 赵财胜, 杨富全, 李厚民. 2005. 大陆动力学演化与成矿研究:历史与现状兼论华南地区在地质历史演化期间大陆增生与成矿作用[J]. 矿床地质, 24(3): 193-205.
- 莫宣学, 潘桂棠. 2006. 从特提斯到青藏高原形成:构造-岩浆事件的约束[J]. 地学前缘, 13(6): 43-51.
- 聂飞, 董国臣, 莫宣学, 赵志丹, 王鹏, 崔子良, 范文玉, 刘书生. 2015. 云南保山西邑铅锌矿床硫铅同位素地球化学特征研究[J]. 岩石学报, 31(5): 1327-1334.
- 庞绪成, 朱浩锋, 瑞忠, 宗静. 2010. 新疆包尔图铜矿稀土元素地球化学特征及其地质意义[J]. 中国地质, 37(6): 1699-1709.
- 陶琰, 胡瑞忠, 朱飞霖, 马言胜, 叶霖, 程增涛. 2010. 云南保山核桃坪铅锌矿成矿年龄及动力学背景分析[J]. 岩石学报, 26(6): 1760-1772.
- 王长明, 张寿庭, 邓军, 刘建明. 2007. 内蒙古黄岗梁锡铁多金属矿床层状夕卡岩的喷流沉积成因[J]. 岩石矿物学杂志, 26(5): 409-417.
- 王立强, 程文斌, 罗茂澄, 向浩予. 2012. 西藏蒙亚啊铅锌矿床金属硫化物、石英稀土元素组成特征及其成因研究[J]. 中国地质, 39(3): 740-749.
- 王中刚, 于学元, 赵振华. 1989. 稀土元素地球化学[M]. 北京: 科学出版社, 1-11.
- 吾守艾力·肉孜, 梁生贤, 邹光富, 罗茂金. 2015. AMT与重力方法在云南芦子园地区隐伏岩体勘查中的应用[J]. 物探与化探, 39(3): 525-529.
- 夏庆霖, 陈永清, 卢映祥, 蒋成兴, 刘红光, 吕志成. 2005. 云南芦子园铅锌矿床地球化学、流体包裹体及稳定同位素特征[J]. 地球科学, 30(2): 177-186.
- 向世红, 薛春纪, 曹纪虎, 张旭, 李永峰, 李丙奇. 2013. 河南内乡北部铅锌银矿方解石的碳-氧同位素特征及地质意义[J]. 矿物岩石地球化学通报, 32(3): 364-369.
- 肖昌浩. 2013. 三江中南段低温热液矿床成矿系列研究[D]. 北京: 中国地质大学, 1-153.
- 杨飞. 2015. 云南省镇康县嗡空铅锌矿成矿地质背景及矿床地质特征[D]. 北京: 中国地质大学, 1-59.
- 杨向荣, 彭建堂, 胡瑞忠, 戚华文, 刘燊. 2009. 新疆塔里木盆地西南缘塔木铅锌矿床矿石管状构造特征与成因[J]. 岩石学报, (4): 977-983.
- 禹丽, 李龚健, 王庆飞, 刘学飞. 2014. 保山地块北部晚白垩世岩浆岩成因及其构造指示:全岩地球化学、锆石U-Pb年代学和Hf同位素制约[J]. 岩石学报, 30(9): 2709-2724.
- 袁波, 毛景文, 闫兴虎, 吴越, 张锋, 赵亮亮. 2014. 四川大梁子铅锌矿成矿物质来源与成矿机制:硫、碳、氢、氧、锶同位素及闪锌矿微量元素制约[J]. 岩石学报, 30(1): 209-220.
- 张传昱, 李文昌, 余海军, 李婉婷, 罗建宏, 沙建泽, 吴清华, 潘泽伟. 2022. 云南水头山铅锌矿床闪锌矿Rb-Sr定年及其地质意义[J]. 沉积与特提斯地质, 42(1): 122-132.
- 章永梅, 顾雪祥, 彭义伟, 郑硌, 张岩, 高海军, 董树义. 2014. 安哥拉Bonga碳酸岩型铌矿床地质地球化学特征及成因[J]. 地学前缘, 21(5): 50-68.
- 周家喜, 黄智龙, 周国富, 金中国, 李晓彪, 丁伟, 谷静. 2010. 黔西北赫章天桥铅锌矿床成矿物质来源: S、Pb同位素和REE制约[J]. 地质论评, 56(4): 513-524.
- 周家喜, 黄智龙, 周国富, 曾乔松. 2012. 黔西北天桥铅锌矿床热液方解石C、O同位素和REE地球化学[J]. 大地构造与成矿学, 36(1): 93-101.